AD-A151 428 MODIFICATIONS TO A PROPAGATION MODEL FOR THE COMBINDED REFRACTION-DIFFRAC.. (U) FLORIDA UNIV GAINESVILLE DEPT OF COASTAL AND OCEANOGRAPHIC EN.. J T KIRBY ET AL. 1/1

UNCLASSIFIED JAN 85 UFL/COEL-85/001 N00014-84-C-0188 F/G 20/4 NL

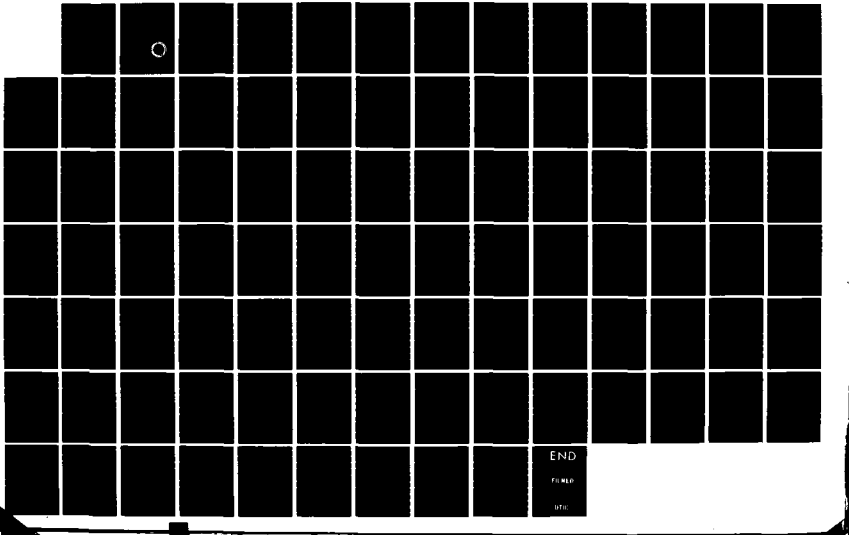

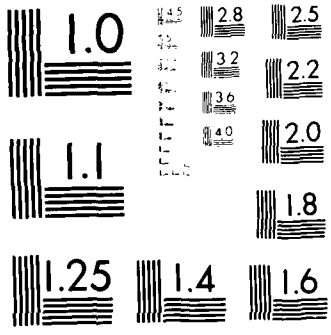

AD-A151 428

UFL/COEL-85/001

MODIFICATIONS TO A PROPAGATION MODEL FOR THE COMBINED REFRACTION-DIFFRACTION OF STOKES WAVES;

Shallow Water, Large Angle and Breaking Wave Effects

BY

JAMES T. KIRBY

AND

ROBERT A. DALRYMPLE

JANUARY 1985

COASTAL & OCEANOGRAPHIC ENGINEERING DEPARTMENT

UNIVERSITY OF FLORIDA

Gainesville, Florida 32611

Modifications to a Propagation Model for the Combined Refraction-Diffraction of Stokes Waves: Shallow Water, Large Angle and Breaking Wave Effects

by

James T. Kirby and Robert A. Dalrymple*

Coastal and Oceanographic Engineering Department

University of Florida, Gainesville, FL 32611

Research Sponsored by the

Office of Naval Research, Coastal Sciences Program

Grant No.: N00014-84-C-0188

January, 1985

*Department of Civil Engineering
University of Delaware
Newark, DE 19716

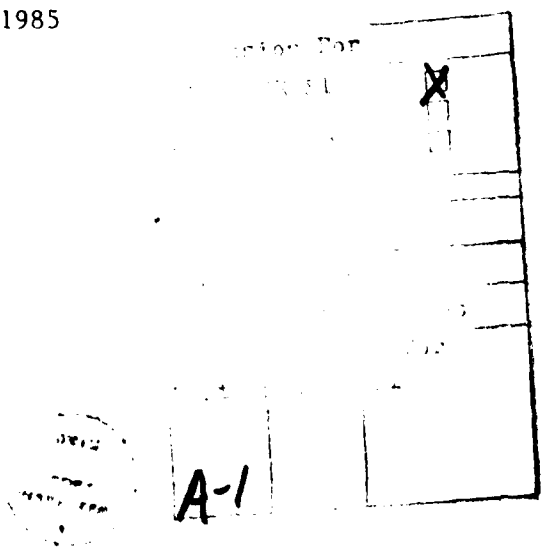

REPORT DOCUMENTATION PAGE

1. Report No.	2.	3. Recipient's Accession No.
UFL/COEL-85/001		

4. Title and Subtitle	5. Report Date
Modifications to a Propagation Model for the Combined Refraction-Diffraction of Stokes Waves: Shallow Water, Large Angle and Breaking Wave Effects	January 1985
	6.

7. Author(s)	8. Performing Organization Report No.
James T. Kirby and Robert A. Dalrymple*	UFL/COEL-85/001

9. Performing Organization Name and Address	10. Project/Task/Work Unit No.
Coastal and Oceanographic Engineering Department 336 Weil Hall University of Florida Gainesville, FL 32611	11. Contract or Grant No. N00014-84-C-0188

12. Sponsoring Organization Name and Address	13. Type of Report
Office of Naval Research, Arlington, VA. subcontract through University of Delaware, Newark, DE 19711	Miscellaneous Report
	14.

15. Supplementary Notes

16. Abstract

This report discusses several features of the combined refraction-diffraction model for Stokes waves (developed by Kirby, 1983) which limit its applicability in shallow water. Chapter 2 discusses a proposed dispersion relation for waves in arbitrary water depth, which provides a smooth patch between the lowest order Stokes dispersion relation and an approximate dispersion relation for shallow water, given originally by Hedges (1976). Chapter 3 extends the large-angle approximation of Kirby (1983) to the case of waves on currents, in order to allow for the calculation of waves which are refracted or diffracted to angles which deviate significantly from an initially preferred direction of propagation, due to the combined effect of varying depth and current. Finally, Chapter 4 provides some calculations of wave fields around surface-piercing islands, in order to illustrate the effect of wave breaking and the use of a thin-film approximation for dry areas in the model.

17. Originator's Key Words	18. Availability Statement
Parabolic equation method combined refraction-diffraction numerical wave model nonlinear waves	distribution unlimited

19. U. S. Security Classif. of the Report	20. U. S. Security Classif. of This Page	21. No. of Pages	22. Price
unclassified	unclassified		

ABSTRACT

This report discusses several features of the combined refraction-diffraction model for Stokes waves (developed by Kirby, 1983) which limit its applicability in shallow water. Chapter 2 discusses a proposed dispersion relation for waves in arbitrary water depth, which provides a smooth patch between the lowest order Stokes dispersion relation and an approximate dispersion relation for shallow water, given originally by Hedges (1976). Chapter 3 extends the large-angle approximation of Kirby (1983) to the case of waves on currents, in order to allow for the calculation of waves which are refracted or diffracted to angles which deviate significantly from an initially preferred direction of propagation, due to the combined effect of varying depth and current. Finally, Chapter 4 provides some calculations of wave fields around surface-piercing islands, in order to illustrate the effect of wave breaking and the use of a thin-film approximation for dry areas in the model.

ACKNOWLEDGEMENT

The work described in this report represents a further step in the continuing development of models for slowly varying wave trains through regions of varying depth and current. The authors wish to thank the Office of Naval Research, Coastal Sciences Program for its continuing support of this work. Special thanks are also extended to Subarna B. Malakar for help with programming and to Jean Branson for preparation of the final typescript. This work was performed under grant N00014-84-C-0188 from the Office of Naval Research, through a subcontract with the University of Delaware, Newark, Delaware.

TABLE OF CONTENTS

LIST OF FIGURES

List of Figures Cont'd.

Chapter 1. Introduction

Recently, a series of papers and reports (Yue and Mei, 1980; Kirby, 1983, 1984; Kirby and Dalrymple, 1983a,b, 1984; Liu and Tsay, 1984) have detailed the derivation of a parabolic model for the forward scattered component of a train of time-periodic, weakly nonlinear Stokes waves. In its most general form, the model is applicable to the study of wave propagation through regions with both slowly varying depth and ambient currents. For the case without currents, good agreement between experiment and theory has been demonstrated (Kirby and Dalrymple, 1984 and Liu and Tsay, 1984) for cases where Stokes theory is strictly valid.

The development of a wave model designed for practical application to realistic modelling problems poses a number of physical problems which do not fit within the theoretical context of the Stokes wave model. Several of these problems are discussed in the present report, and methods for including their effects in the combined refraction-diffraction model are proposed.

In Chapter 2, the problem of matching dispersion relations between Stokes and shallow water waves is discussed, and a formulation is proposed which smoothly matches the dispersion relation for Stokes waves to an approximate dispersion relation due to Hedges (1976) for shallow water. The proposed matching alleviates the need for extending approximate calculations into deeper water when their use in shallower water is dictated. Further, the provision of a continuously-varying formula for all water depths insures a smooth variation in both phase and group velocities from deep to shallow water, eliminating the regions of discontinuity between Stokes theory and the full cnoidal wave theory.

In Chapter 3, a formulation for waves propagating at not-so-small angles to the preferred direction and in the presence of an ambient current is given in full. The present derivation follows the scheme indicated by Kirby (1983), but the material presented here was not pursued to the point of completeness in the former report.

Finally, Chapter 4 presents an application of the breaking wave model described by Kirby (1983) and Dally, Dean and Dalrymple (1984) to the case of a surf zone around an island. Since this chapter is in the form of a full manuscript, discussion of the physical problem is left to the chapter introduction.

Chapter 2. A Modification of the Nonlinear Dispersion Relation for Shallow Water Waves

A central problem in present efforts at modelling waves in coastal regions consists of the mismatch in wave properties as waves propagate from an intermediate depth region, in which Stokes theory is valid, into the nearshore zone, where waves are better described by the Boussinesq equations. Several theories for large amplitude waves in arbitrary depth (Dean, 1965; Rienecker and Fenton, 1981, for example) provide a bridge across the division between Stokes theory and cnoidal theory; these theories are computationally intensive and are typically used to accurately describe the properties of a single wave. For the computation of waves propagating through large areas of variable depth, the use of the theories for waves of small amplitude is computationally more feasible at present; formulations of this type are the subject of the present report.

2.1. Review of Stokes Theory

Recently, progress has been made in modelling the propagation of small amplitude Stokes waves due to the simplicity of the dispersion relation incorporating the lowest-order nonlinearity. Following Whitham (1967), this relation may be written as

$$\omega^2 = \omega_0^2\left(1 + (ka)^2 D(kh)\right) \tag{2.1}$$

where

$$\omega_0^2 = gk\tanh kh \tag{2.2}$$

is the linear dispersion relation, and where

$$D(kh) = \frac{\cosh(4kh) + 8 - 2\tanh^2(kh)}{8\sinh^4(kh)} \qquad (2.3)$$

(2.1) may be used to determine either ω or k given a, the local wave amplitude, and h. Yue and Mei (1980) demonstrated that (2.3) may be incorporated in the lowest order parabolic approximation of the Helmholtz equation, yielding

$$2ik_o A_x + A_{yy} - \frac{\omega k_o^3}{C_g} D|A|^2 A = 0 \qquad (2.4)$$

where A is the complex amplitude of a wave described by

$$\eta = \mathrm{Re}\{Ae^{i[k_o x - \omega t]}\}$$

The resulting equation is in the form of a cubic Schrödinger equation for wave evolution in the x-direction. This formulation has been extended to the case of waves on currents in a slowly varying domain, yielding the equation (Kirby; 1983, 1984):

$$(C_g + U)A_x + VA_y + \frac{\sigma}{2}\left\{\left[\frac{C_g + U}{\sigma}\right]_x + \left[\frac{U}{\sigma}\right]_y\right\}A$$

$$- \frac{i}{2\sigma}(CC_g A_y)_y - \sigma k^3 D|A|^2 A = 0 \qquad (2.5)$$

where

$$\sigma = \omega + kU, \qquad (2.6)$$

$$\omega = (gk\tanh kh)^{1/2} \qquad (2.7)$$

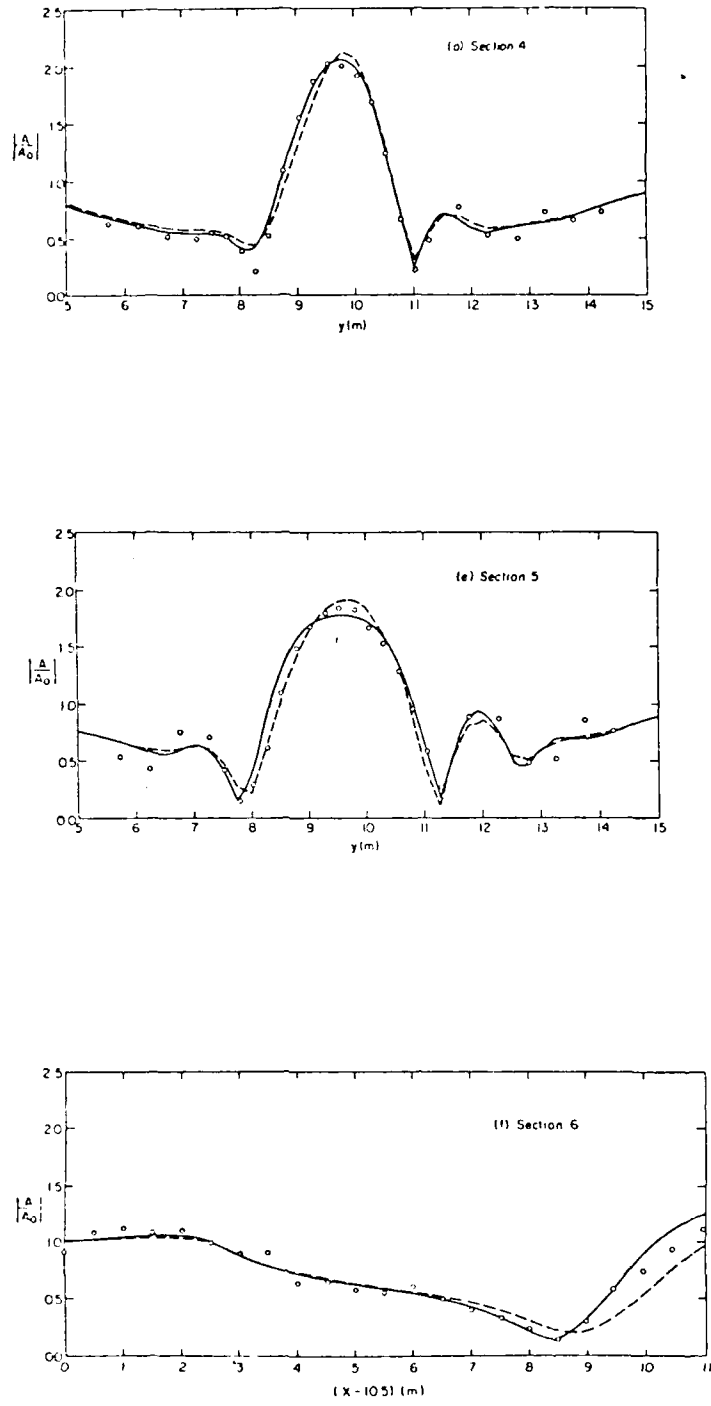

Figure 2.4.

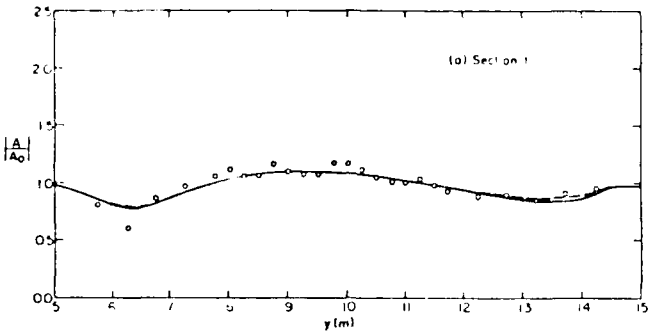

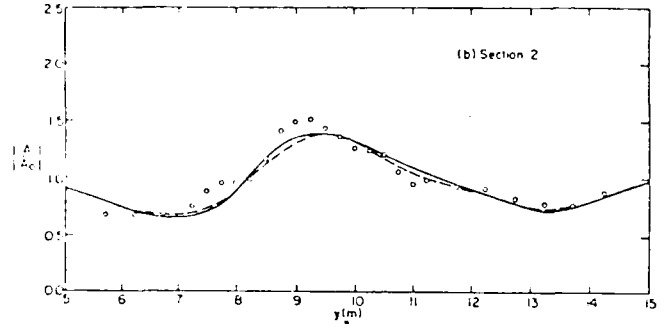

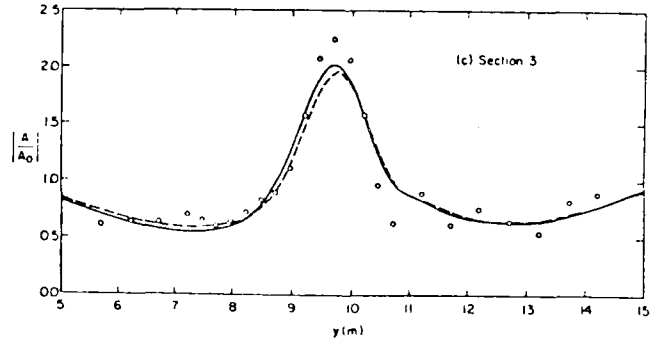

Figure 2.4.

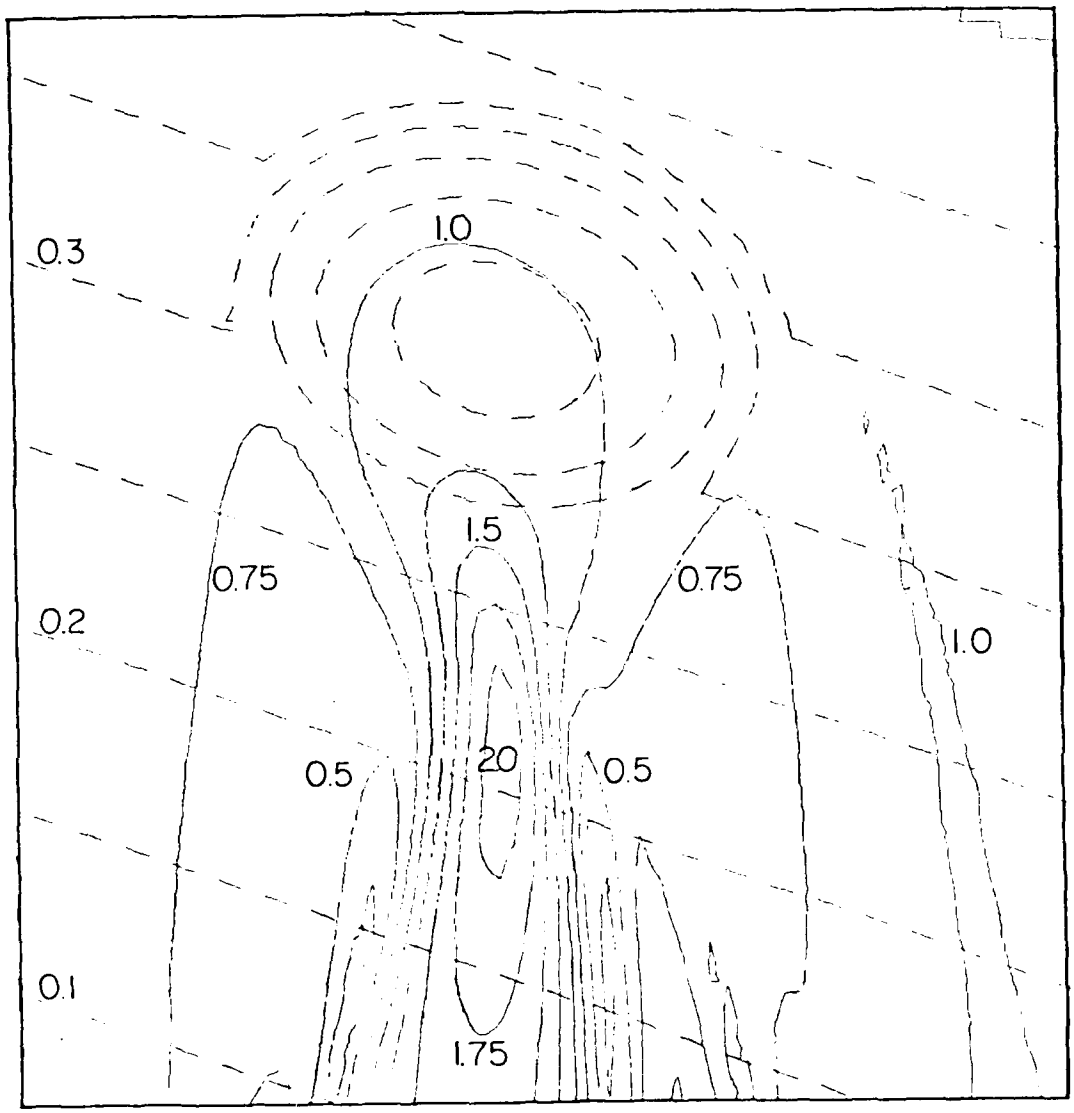

Figure 2.3. Amplitude contours relative to incident wave amplitude: Hedges (1976) approximate formulation.

$$A_y = 0; \text{ lateral boundaries} \qquad (2.28)$$

The computational model used in the present examples is obtained from (3.28 - 29) by setting $\underset{\sim}{U} = (U,V) = 0$, neglecting any imposed ambient current. We further adopt the lower order approximation of Radder (1979) and set $P_1 = 0$ in (3.28).

Data from the laboratory experiment of Berkhoff et al (1982) are available for the labelled transects 1 through 8 indicated in Figure 2.2. The computational domain was discretized into square grids $\Delta x = \Delta y$ = grid spacing), and the grid scheme was established so that grid rows coincided with the measurement transects. Grid size was decreased until the point was reached where further reduction did not affect model predictions significantly. The final numerical calculations were performed using a space of $\Delta x = 0.25$ m. Results for wave amplitude normalized by the incident wave amplitude are presented in Figure 2.3 in the form of a contour plot for the region of the shoal and focus. The results for the Hedges model are qualitatively similar to the Stokes waves results presented in Kirby and Dalrymple (1984), and agreement between the Stokes and Hedges results is definitely better than between either nonlinear model and linear theory.

Plots of normalized amplitude for the labelled transects 1 - 8 in Figure 2.2 are given in Figures 2.4a - h, respectively. The plots include results of the Hedges model, the Stokes model and the laboratory data of Berkhoff et al (1982).

where A_o = 0.0232 m is the amplitude of the incident wave. The wave period T = 1 sec. Referring to Figure 2.2, we establish slope-oriented coordinates $\{x', y'\}$ which are related to the computational coordinates $\{x,y\}$ according to:

$$x' = (x - 10.5)\cos 20^0 - (y - 10)\sin 20^0 \qquad (2.24a)$$

$$y' = (x - 10.5)\sin 20^0 + (y - 10)\cos 20^0 \qquad (2.24b)$$

The origin $\{x', y'\} = \{0,0\}$ corresponds to the center of the shoal. The slope is described by:

$$h = \begin{cases} 0.45 \text{ m}, & x' < -5.82 \text{ m} \qquad (2.25a) \\ 0.45 - 0.02\,(5.82 + x')\text{m}, & x' \geq -5.82 \text{ m} \qquad (2.25b) \end{cases}$$

The boundary of the elliptic shoal is given by:

$$\left(\frac{x'}{3}\right)^2 + \left(\frac{y'}{4}\right)^2 = 1 \qquad (2.26)$$

and the depth in the shoal region is modified according to:

$$h = h_{slope} - 0.5\left[1 - \left(\frac{x'}{3.75}\right)^2 - \left(\frac{y'}{5}\right)^2\right]^{1/2} + 0.3 \qquad (2.27)$$

resulting in a depth $h(x' = 0, y' = 0) = 0.1332$ m.

The lateral boundaries at y = 0, 20 m are open, but are far enough from the region of the shoal so that we can specify reflective boundary conditions on the lateral boundaries

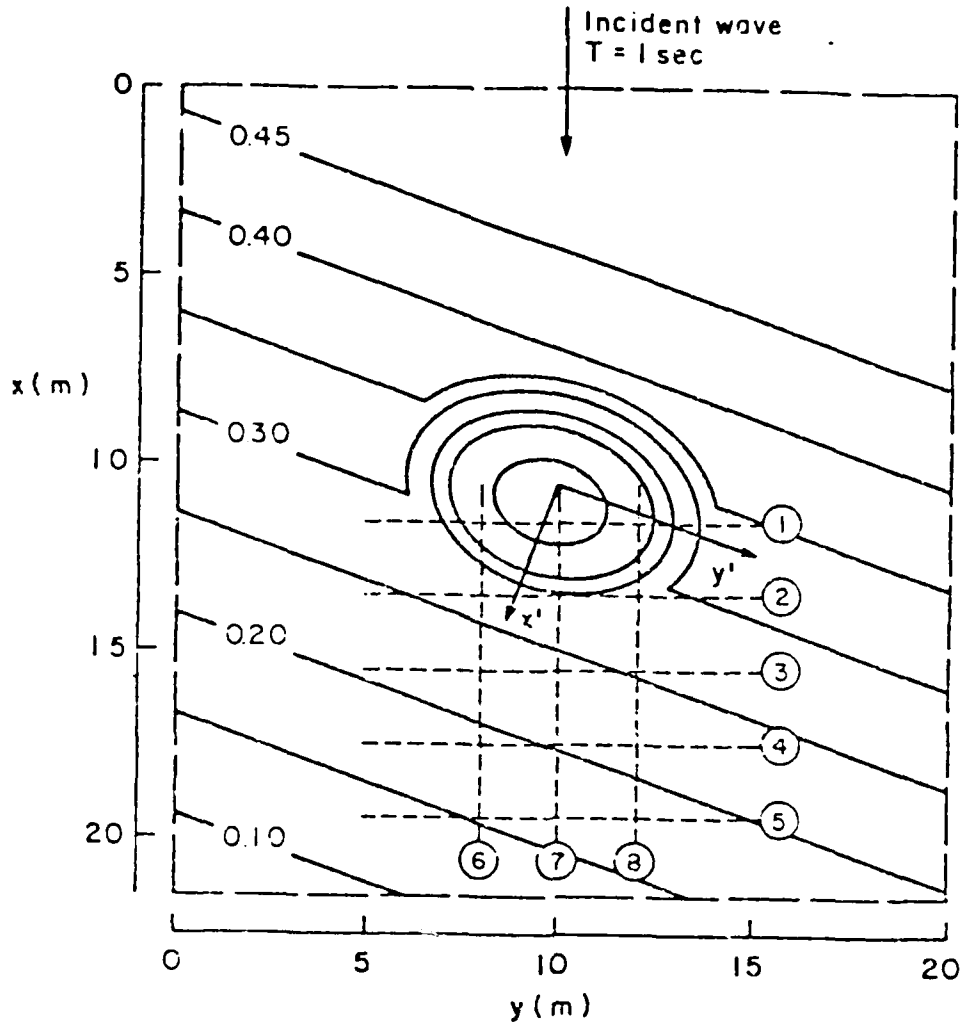

Figure 2.2. Topography and computational domain for experiment of Berkhoff et al. (1982). Dashed lines indicate transects labelled as sections 1-8 in Figures 2.4 and 2.7.

definitive laboratory data which shows the direct effect of amplitude dispersion in intermediate depth. For this reason, we include here a comparison of the refraction-diffraction calculations based on Hedges form of the dispersion relation, and data taken from the experiments described by Berkhoff et al (1982). This data set has already been used to check the linear form of the CREDIZ model (Berkhoff et al, 1982), and a nonlinear model based on the Stokes dispersion relation (Kirby, 1983; Kirby and Dalrymple, 1984). The reader is referred to the previous literature for details of the experiment. The work of Kirby (1983) and Kirby and Dalrymple (1984) compare the Stokes model to results obtained using linear theory, and establishes that the Stokes model provides a detailed, accurate reproduction of the experimental data. We therefore take the view in the remainder of this section that the Stokes wave model represents the "correct" wave model for waves in intermediate water depth ($U_r < O(1)$). We will therefore be primarily interested in how much discrepancy between numerical and experimental results is introduced by using approximate dispersion relations. We summarize the important points of the experimental arrangement here. The experimental topography consists of an elliptic shoal resting on a plane sloping bottom with a slope of 1:50. The plane slope rises from a region of constant depth $h = 0.45$ m, and the entire slope is turned at an angle of 20° to a straight wave paddle. Bottom contours are shown in Figure 2.2 along with the chosen computational domain, which is indicated by the dashed line surrounding the contours. The offshore boundary of the computational domain is chosen so that water depth is constant along $x = 0$. The initial condition for the wave then corresponds to the uniform wave train generated at the wave paddle; we set:

$$A(x = 0, y) = A_0 \tag{2.23}$$

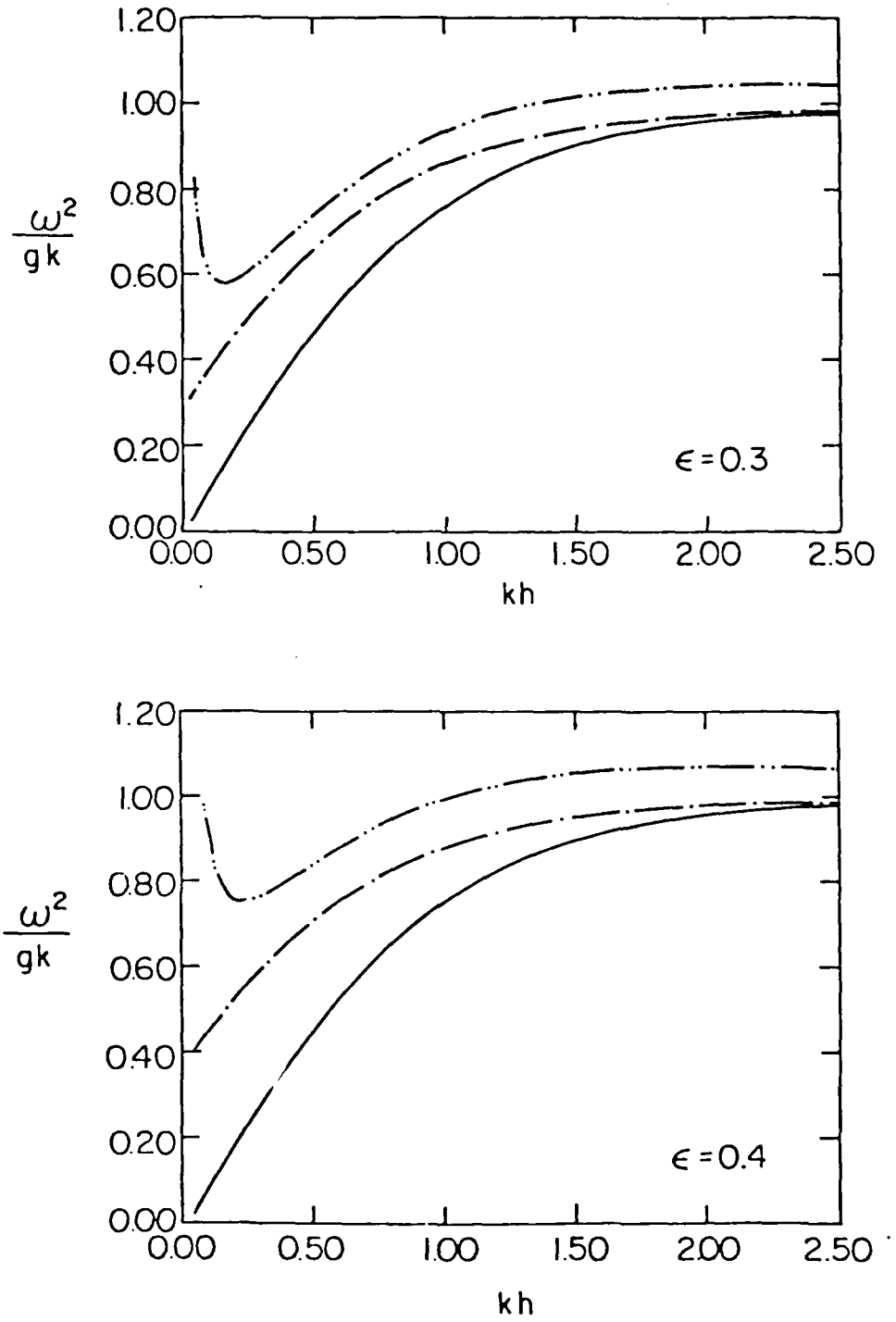

Figure 2.1. (Continued).

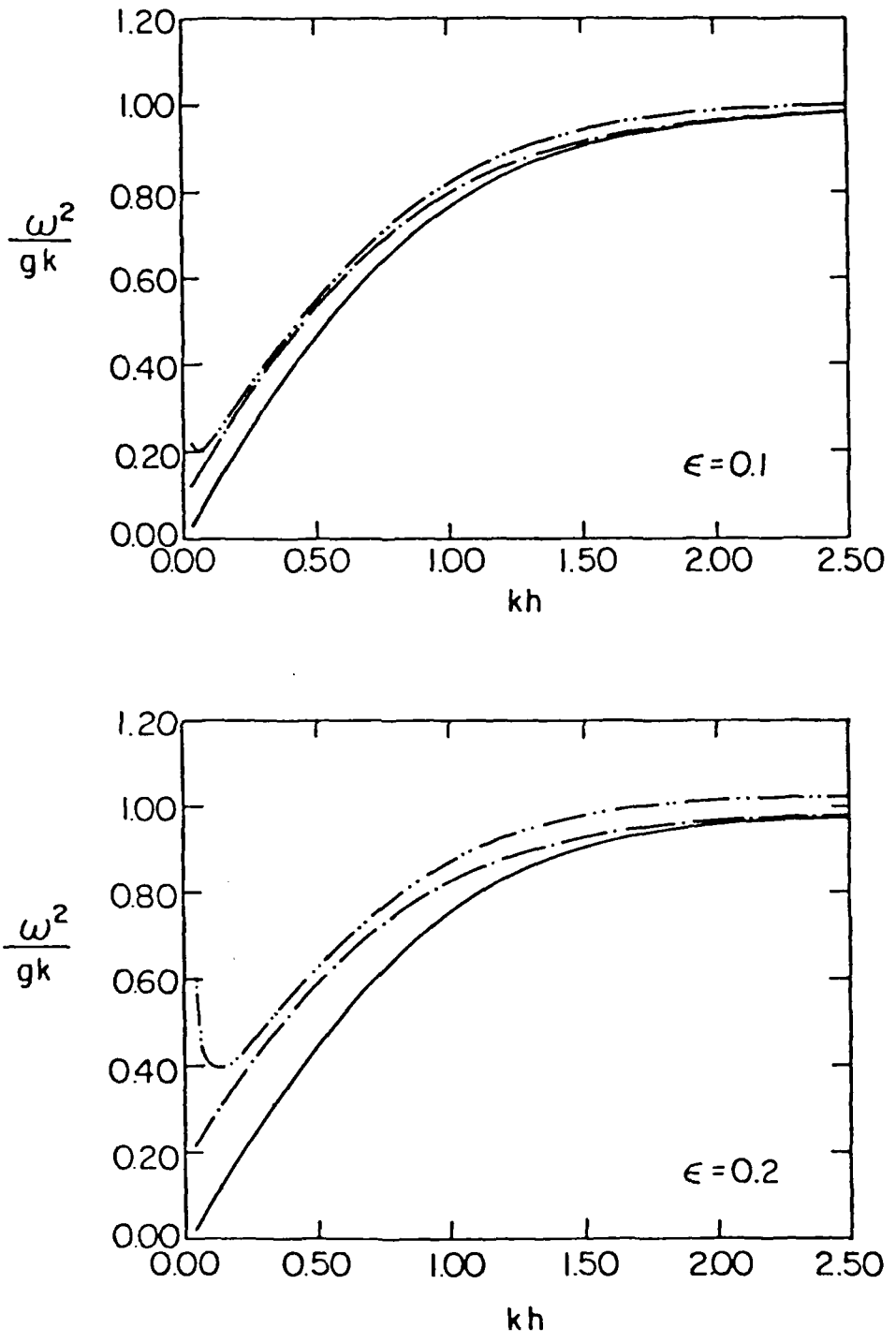

Figure 2.1. Variation of the linear and shallow water approximate dispersion relations with kh and wave steepness ϵ = ka ——— linear; - • - • Hedges (1976); — • • — • • — Walker (1976). a) ϵ = 0.1, b) ϵ = 0.2, c) ϵ = 0.3, d) ϵ = 0.4.

$$\omega^2/gk = (1 + \varepsilon/2kh)\tanh(kh + \varepsilon/2) \qquad (2.20)$$

corresponding to Walker's approximation, and

$$\omega^2/gk = \tanh(kh + \varepsilon) \qquad (2.21)$$

corresponding to Hedges approximation. The variation is over values of kh for fixed values of wave steepness $\varepsilon = ka$; curves are given for values of $\varepsilon = 0.1$, 0.2, 0.3 and 0.4. The results show that the difference between Walker's approximate form and linear theory remains pronounced for large values of kh, while Hedges approximation approaches the linear result move rapidly. The common shallow water limit of the two relations for small a/h is seen to break down for finite values of a/h, with (2.20) reducing to

$$\omega^2/gk = kh + \varepsilon + \varepsilon^2/4kh \qquad (2.22)$$

where the last term becomes large for any fixed ε as $kh \to 0$. It seems that Booij's conclusion that Hedges' approximation is preferable to Walker's based on the deep water behavior extends as well to the shallow water limit, due to the $O(\varepsilon^2)$ term which cannot be made arbitrarily small in shallow water.

Hedges (1976) approximation has been used to form the basis of nonlinear effects in at least one operational refraction-diffraction model; the model CREDIZ developed by the Delft Hydraulics Laboratory in conjunction with the Rijkswaterstaat. A recent calibration of this model is described in Dingemanns (1983) and Dingemanns et al (1984). To date, no adequate comparison has been made between the approximate nonlinear model and any

Alternatively, Hedges (1976) proposed a similar relation of the form

$$\omega^2 = gk \tanh(k[h + a]) \qquad (2.16)$$

Both (2.15) and (2.16) have similar properties in the limits of deep and shallow water. In shallow water and for a/h small, both formulas lead to a dispersion relation

$$\omega^2 = gk^2(h + a) \qquad (2.17)$$

or, equivalently, a phase speed

$$C = [g(h + a)]^{1/2} \qquad (2.18)$$

This phase speed represents the speed of propagation of a solitary wave of height H = 2a. The shallow limit of either approximate form is thus physically reasonable.

In the deep water limit, both (2.15) and (2.16) approach the linear dispersion relation, as the ratio a/h approaches zero due to increasing water depth. Booij (1981) has mentioned, without demonstration, that the approach to the linear form is quite slow if the relation (2.15) of Walker is used. Figure 2.1 shows the variation of the right-hand side of the relations

$$\frac{\omega^2}{gk} = \tanh kh \qquad (2.19)$$

corresponding to linear theory,

Recently, Liu et al (1985) have shown that refraction-diffraction calculations may be performed for regular cnoidal waves using a spectral approach based on the Boussinesq equation. This method is reasonably simple to develop, and computations are straight forward and fairly economical due to the simplicity of the wave-wave interaction coefficients in shallow water. However, the calculations are highly dependent on the relative phase speeds and amplitudes of a number of waves in a discrete spectrum, and the method can not be applied to the present monochromatic model.

Alternatively, several authors have proposed simple modifications to the linear dispersion relation which are designed to mimic the effect of amplitude dispersion in shallow water. Based on a large number of laboratory observations of broken and unbroken waves propagating over a focusing topography, Walker (1976) proposed that the nonlinear effects in shallow water could be modelled in a refraction scheme by modifying the predicted linear phase speed according to

$$C_{n\ell} = C_{\ell}(1 + a/h) \tag{2.13}$$

where "a" is the wave amplitude and

$$C_{\ell} = \frac{\omega}{k} = (g\tanh kh/k)^{1/2} . \tag{2.14}$$

Booij (1981) showed that a dispersion relation equivalent to (2.13) may be written as

$$\omega^2 = gk\left(1 + \frac{a}{2h}\right) \tanh\left(k\left[h + \frac{a}{2}\right]\right) \tag{2.15}$$

2.2. Approximate Shallow Water Dispersion

The limitations of the Stokes theory leads to two modelling problems:

1) An alternate theory (cnoidal waves) must be used to describe waves in the range where

$$\frac{|A|/h}{(kh)^2} \sim O(1);$$

2) A way must be found to describe the smooth transition of waves from the Stokes regime into the cnoidal regime.

The first problem results from the limits of validity of the Stokes theory. The second problem arises due to the fact that wave properties do not vary smoothly across the division between Stokes and cnoidal waves.

Using the results of cnoidal wave theory, the dispersion relation for periodic waves may be written as (Flick, 1978)

$$C = (gh)^{1/2} \left(1 + \frac{|A|}{h} f_1(m)\right) \qquad (2.11)$$

where

$$f_1(m) = \frac{1}{m}\left(2 - \frac{3E(m)}{K(m)} - m\right) \qquad (2.12)$$

and where E(m) and K(m) are the Jacobean elliptic integrals.

This relation may be used to calculate local values of k in a modelling scheme. This analytic approach has been used in several refraction schemes (Chu, 1975; Skovgaard and Petersen, 1977; Headland and Chu, 1984) as a means for including the effect of shallow water amplitude dispersion. The full formulation requires a large amount of iterative computation due to the interrelationship of the wave height H and elliptic parameter m.

Here, ω is the fixed wave frequency with respect to the stationary domain, and the wave is assumed to be propagating in the x-direction.

Equations of the form (2.5) (or the large angle, large current extension described in Chapter 3) are applicable in intermediate depth $(kh \sim 0(1))$ and are correct in the deep water asymptote $(kh \to \infty)$ under the condition of $k|A| \ll 1$. In shallow water, the regular expansion in $k|A|$ breaks down and is replaced instead by an expansion to lowest order in $kh \ll 1$, $|A|/h \ll 1$, with the Ursell number

$$U_r = \frac{|A|/h}{(kh)^2} \sim 0(1) \tag{2.8}$$

representing the region where cnoidal and solitary waves are described. The breakdown in the Stokes theory may be seen by looking at the shallow limit of (2.3);

$$D(kh) \sim \frac{9}{8}(kh)^{-4}; \quad kh \to 0 \tag{2.9}$$

The singularity in D as $kh \to 0$ is quite severe and overwhelms the computations if regions of the computational domain become too shallow. The dispersion relation may be arranged to the form

$$\omega^2 \simeq \omega_o^2\left(1 + \frac{9}{8}\left(\frac{|A|}{h}\right)^2 (kh)^{-2}\right) \tag{2.10}$$

indicating that $|A|/h$ must remain extremely small as $kh \to 0$, in order for the Stokes theory to remain valid. This requirement is clearly not applicable in the vicinity of surfzones, where $|A|/h$ is typically of $0(1)$.

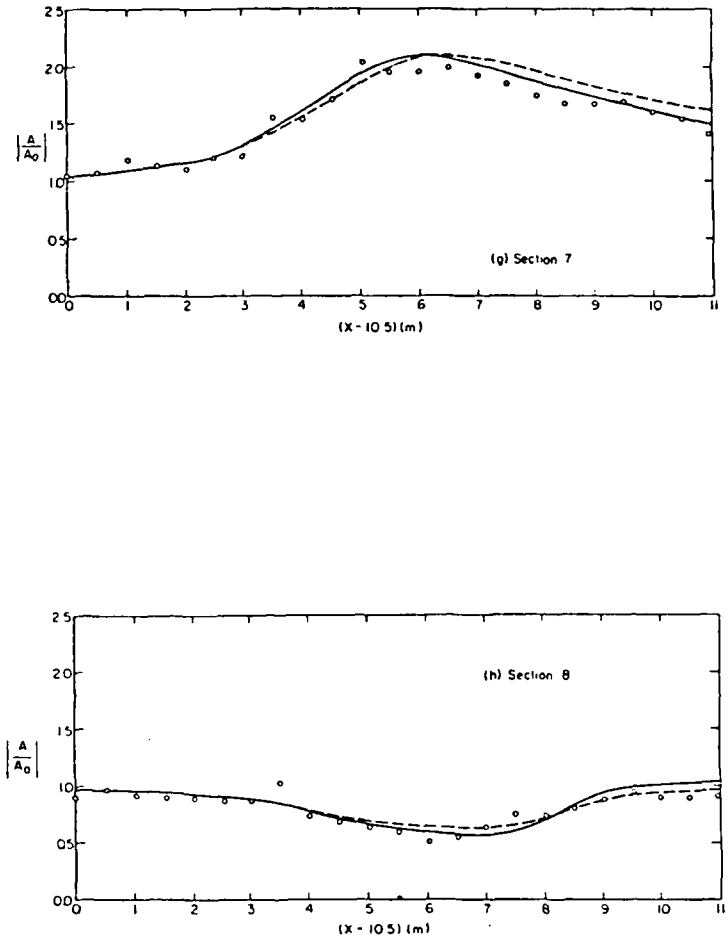

Figure 2.4. Comparison of model using Hedges (1976) dispersion relation to the Stokes model (Kirby and Dalrymple, 1984) and laboratory data (Berkhoff et al., 1982). ——— Stokes model; ----- Hedges model; o laboratory data. a-h) sections 1-8, respectively.

2.3. Matching Stokes and Shallow Water Dispersion

The inadequacy of an approximate shallow water dispersion to model nonlinear effects in intermediate water depth, coupled with the invalidity of the Stokes model in shallow water, leads to the need for a matched dispersion relation which predicts the phase speeds of waves smoothly from deep to shallow water. This problem is central to the prediction of the properties of shoaling waves.

Goring (1978) has shown that a matching exists between Stokes and cnoidal waves in the limit of small amplitude, by showing that a regular perturbation solution of the Korteweg-deVries equation is equivalent to the shallow water limit of the Stokes solution for general water depth. However, for larger amplitudes the series solution does not converge, and the solution in terms of powers of $\varepsilon = ka$ becomes inappropriate. In effect, as water depth decreases, the Stokes solution may become invalid before the region of validity of the cnoidal theory (small kh) is reached. Flick (1978) suggested that it may be possible to construct a dispersion relation by means of matched asymptotic expansions; he suggests a relation of the form

$$C = \frac{\omega}{k} = C_s + C_c - C_{\ell in} \tag{2.29}$$

where

$$C_s = (1 + \varepsilon^2 D)^{1/2} \, (g \tanh kh/k)^{1/2} \tag{2.30}$$

is the Stokes phase speed,

$$C_c = (gh)^{1/2}\left(1 + \frac{a}{h} f_1(m)\right)$$

$$f_1(m) = (2 - 3E/m)/K(m) - m)/m \qquad (2.31)$$

is the cnoidal phase speed, and

$$C_{\ell in} = (gh)^{1/2}\left(1 - \frac{1}{6}(kh)^2 + \frac{9}{16}\left[\frac{a/h}{(kh)^2}\right]^2\right) \qquad (2.32)$$

is both the shallow water limit of (2.30) and the small amplitude ($m \to 0$) limit of (2.31). The fact that these limits coincide lends further creedence to the conclusions of Goring (1978). However, in cases where the small-amplitude limit is inappropriate, (2.32) may not be used directly as a reasonable approximation. This would seemingly include the majority of cnoidal wave cases, where the Ursell parameter $(a/h)/(kh)^2$ is O(1).

For the purpose of inclusion in the monochromatic wave model, we propose that a dispersion relation of the form

$$\omega^2 = gk\left(1 + f_1(kh)\varepsilon^2 D\right) \tanh\left(kh + f_2(kh)\varepsilon\right) \qquad (2.33)$$

may be constructed in order to model nonlinear effects over a broad range of depths. Comparing (2.33) to the previous forms of the dispersion relation, we see that the Stokes wave form is recovered by the choice

$$\begin{aligned} f_1(kh) &= 1. \\ &\qquad \text{all } kh \\ f_2(kh) &= 0. \end{aligned} \qquad (2.34)$$

while the Hedges model is recovered by choosing

$$f_1(kh) = 0. \qquad \text{all } kh \qquad (2.35)$$

$$f_2(kh) = 1.$$

The composite model may be constructed by choosing forms for the arbitrary functions f_1 and f_2. In particular, we require that $f_1(kh) \to 1$ as $kh \to \infty$ while $f_2(kh) \to 0$ as $kh \to \infty$, in order to recover the Stokes wave limit. In shallow water, we require $f_2 \to 1$ as $kh \to 0$, while $f_1(kh)$ must be of $O(kh^5)$ or smaller in order to overcome the singularity in D, which is $O(kh^{-4})$. Based on these requirements, we have chosen f_1 and f_2 according to

$$f_1(kh) = \tanh^5 kh \qquad (2.36)$$

$$f_2(kh) = [kh/\sinh(kh)]^4 \qquad (2.37)$$

The dispersion relation resulting from these choices is illustrated in Figure 2.5, where the right-hand sides of the following relations are plotted.

Linear

$$\frac{\omega^2}{gk} = \tanh kh \qquad (2.38)$$

Stokes

$$\frac{\omega^2}{gk} = (1 + \varepsilon^2 D)\tanh kh \qquad (2.39)$$

Hedges

$$\frac{\omega^2}{gk} = \tanh(kh + \varepsilon) \qquad (2.40)$$

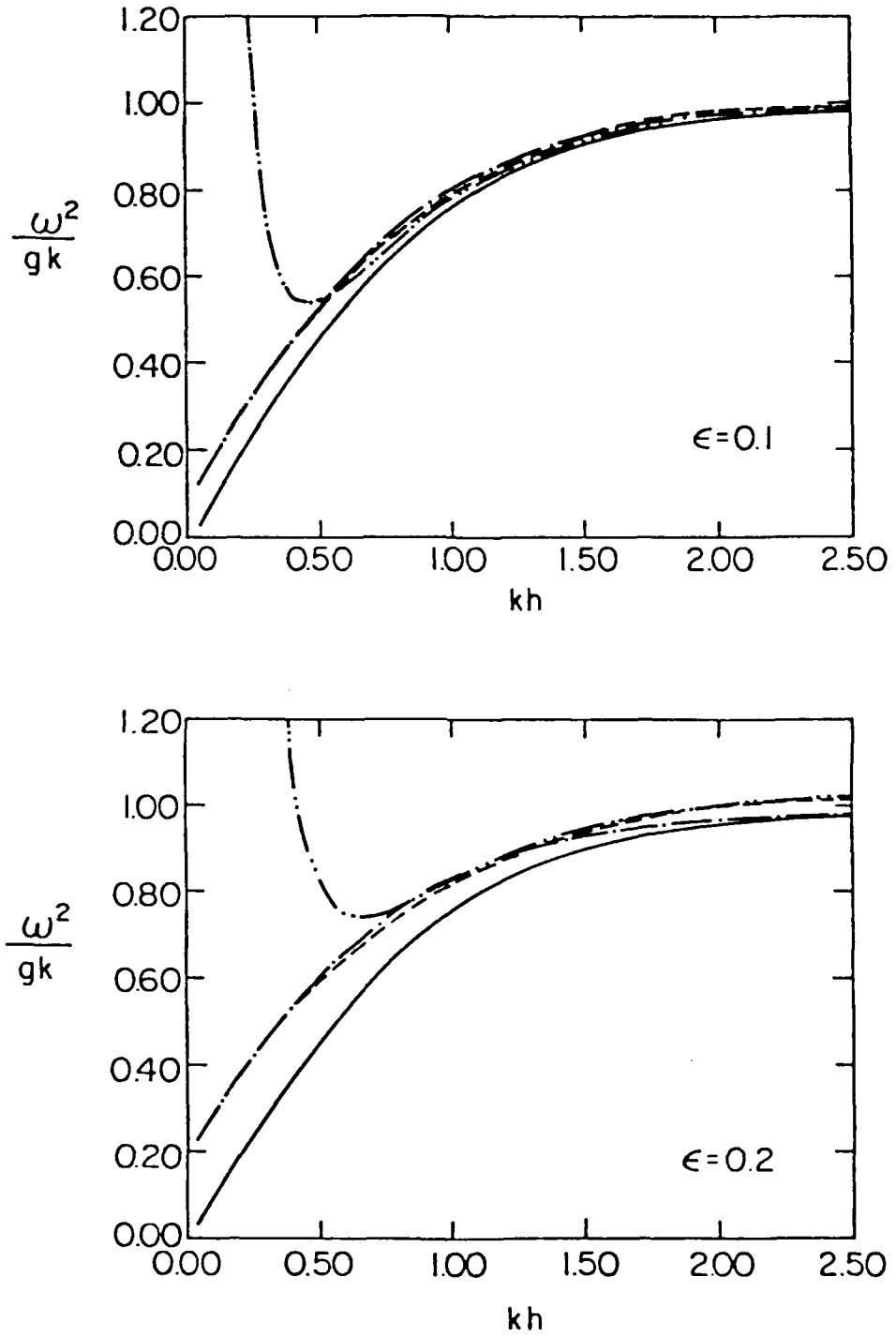

Figure 2.5. Variation of linear and nonlinear dispersion relations with kh and wave steepness $\varepsilon = ka$. ——— linear; —•—•— Hedges; —••—••— Stokes; ----- present composite model. a) $\varepsilon = 0.1$, b) $\varepsilon = 0.2$, c) $\varepsilon = 0.3$, d) $\varepsilon = 0.4$.

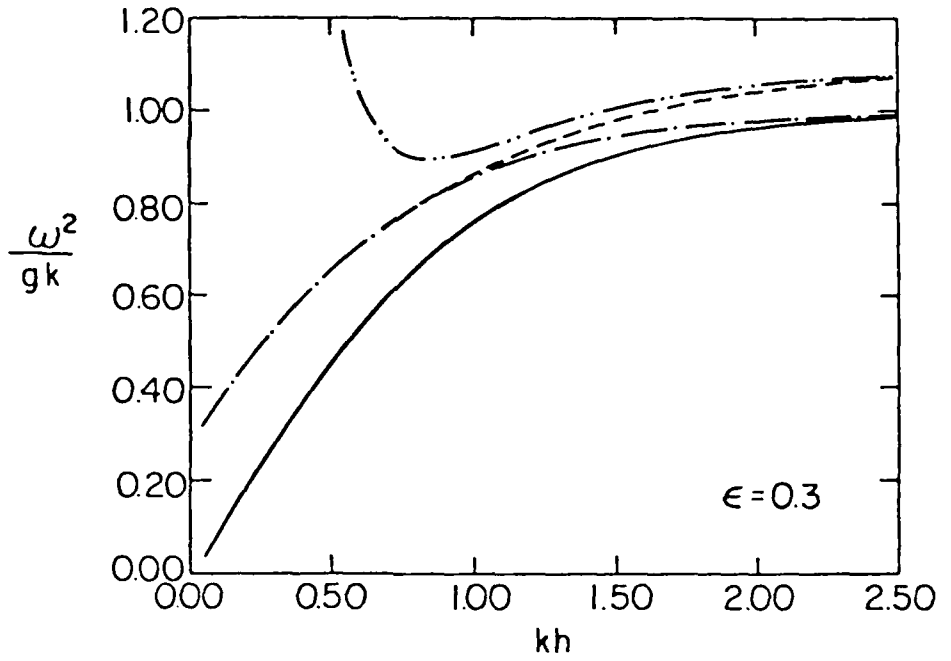

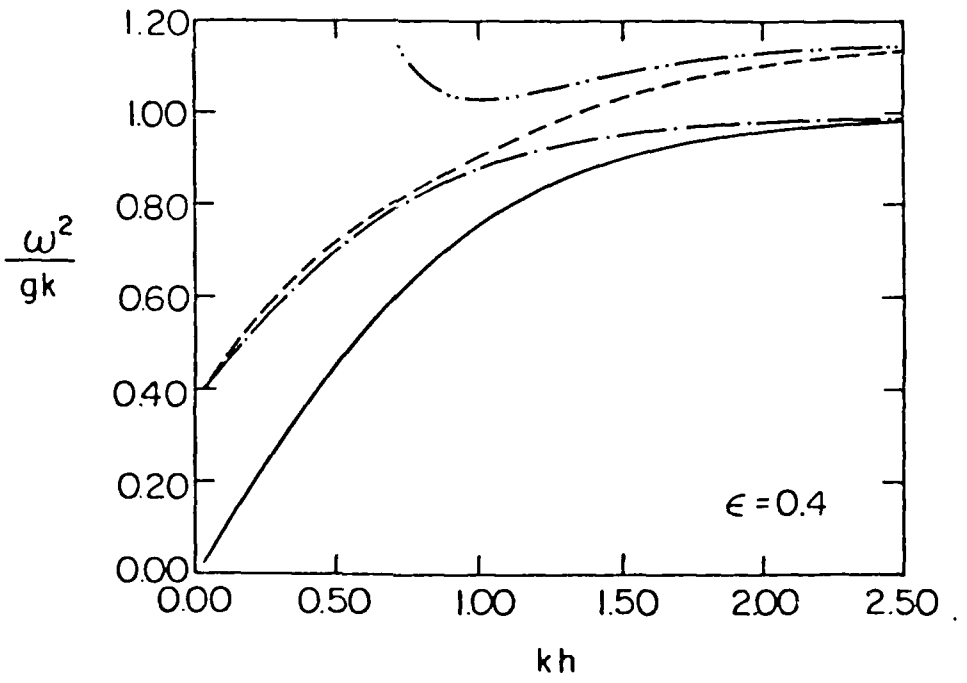

Figure 2.5. (Continued).

$$\text{Composite} \quad \frac{\omega^2}{gk} = (1 + f_1\varepsilon^2 D)\tanh(kh + f_2\varepsilon) \qquad (2.41)$$

As in Figure 2.1, results are plotted for a range of kh values, and separate sets of curves are given for choices of ε = 0.1, 0.2, 0.3 and 0.4. An inspection of each set of curves shows that the composite form (2.41) matches smoothly to both the Stokes form (2.39) in deeper water and the Hedges form (2.40) in shallow water. The strong singularity in the Stokes form is also apparent. The curve corresponding to the composite form typically lies between the Stokes curve and the Hedges curve, which may or may not intersect each other.

We remark that the choice of the exponent 4 in (2.37) led to the best positioning of the composite curve (2.41) with respect to both the Stokes and Hedges relations, with both higher or lower exponents leading to fairly large deviations over some portion of the range of kh. The choice of the exponent 5 in (2.36) is of course dictated by the requirement imposed by the singularity in D.

The composite model was tested by recomputing the example of Berkhoff et al (1982) using the modified dispersion relation. The dispersion relation is incorporated directly in the nonlinear Schrödinger equation for complex amplitude A following the method of Kirby and Dalrymple (1984). The nonlinear modification to the time-dependent form of the linear mild-slope equation for velocity potential $\tilde{\phi}$ at the free surface is given by

$$\tilde{\phi}_{tt} - \nabla_n \cdot (CC_g \nabla_n \tilde{\phi}) + (\omega^2 - k^2 CC_g)\tilde{\phi} + F\tilde{\phi} = 0 \qquad (2.42)$$

where

$$F = \omega^2 - \omega_o^2 \tag{2.43}$$

and ω_o^2 is the linear wave frequency squared;

$$\omega_o^2 = gk\tanh kh \tag{2.44}$$

Representing ω^2 by (2.33) and letting $\tilde{\phi}$ be represented as

$$\tilde{\phi} = Re\{-\frac{ig}{\omega} A(x,y)e^{i(k_o x - \omega_o t)}, \tag{2.45}$$

where k_o is a reference wave number, reduces (2.42) to the form

$$C_g A_x + iC_g(k_o - k)A + \frac{1}{2}(C_g)_x A - \frac{i}{2\omega_o}\nabla_h \cdot (CC_g\nabla_h A)$$

$$+ \frac{i\omega_o}{2}\left[\left(1 + f_1 k^2|A|^2 D\right)\frac{\tanh(kh + f_2 k|A|)}{\tanh kh} - 1\right] A = 0 \tag{2.46}$$

This form of the nonlinear model is used to compute results corresponding to the experimental data. The computational grid and domain is as described in section 2.2. A parabolic form of (2.46) is obtained by using the scaling assumption

$$|A_x| << O(ik|A|), \tag{2.47}$$

leading to the neglect of the term $(CC_g A_x)_x$ in (2.46). Again, the computational scheme is described in Chapter 3; here we use the choice $P_1 = 0$.

A contour plot of normalized amplitude $|A|/A_o$ is given in Figure 2.6. The contours resul ing from calculations using the composite model are closer

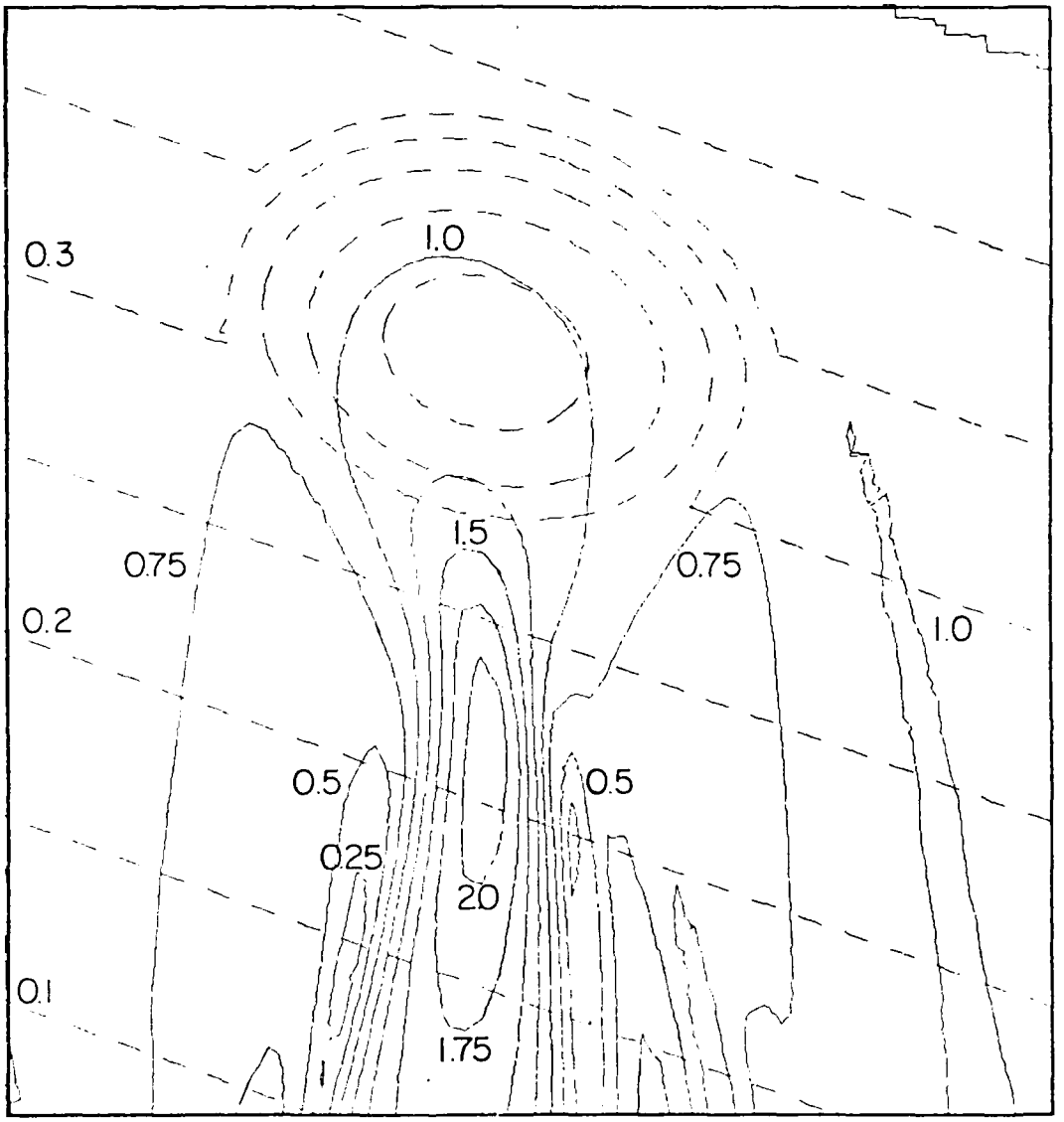

Figure 2.6. Amplitude contours relative to incident wave amplitude: present composite model.

in shape to the results of the Stokes model than are the contours of the Hedges model, as would be expected. Plots of normalized amplitude along the labelled transects 1 - 8 are presented in Figure 2.7, where the composite model results are compared to Stokes model results and laboratory data. The results of the composite model are generally closer to the Stokes model and to the data than are the results of the Hedges model, although the discrepancies in either case are not large, with all models generally showing better agreement with data than the linear model.

2.4 Conclusions

The present chapter has presented a method for extending the effects of nonlinear dispersion in a monochromatic Stokes wave model into water depths which are too shallow for Stokes theory to retain its validity. The proposed model provides a smooth patch between Stokes theory and an empirical shallow water relation due to Hedges, with the two separate forms being obtained in the limit of deep and shallow water, respectively.

Although example calculation show that the differences between the Stokes model and Hedges model are not large in intermediate water depths, we feel that the present results are preferable to the use of the Hedges relation alone for several reasons. First, the fact that the Hedges model approaches a linear model in deep water implies that discrepancies would inevitably exist in calculations which start or extend into fairly deep water. Existing laboratory data covers too shallow a depth range (and too low a range of wave heights) to show these discrepancies fully. The present method provides a means for patching the empirical shallow water model into a more reasonable deep water limit.

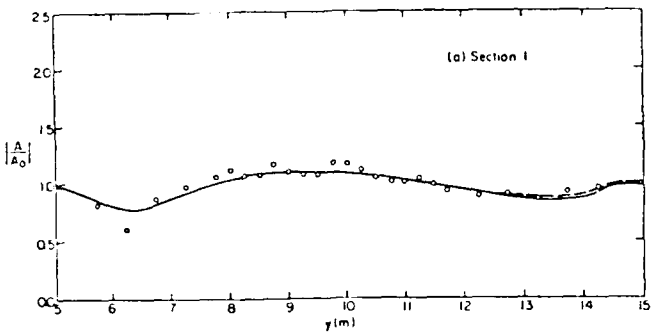

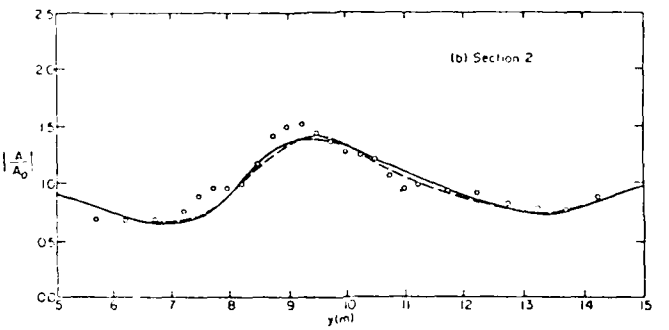

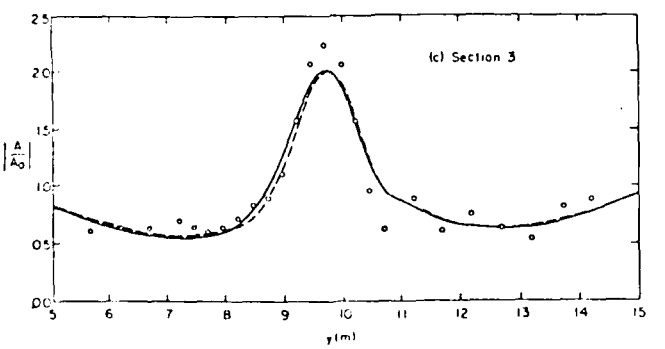

Figure 2.7.

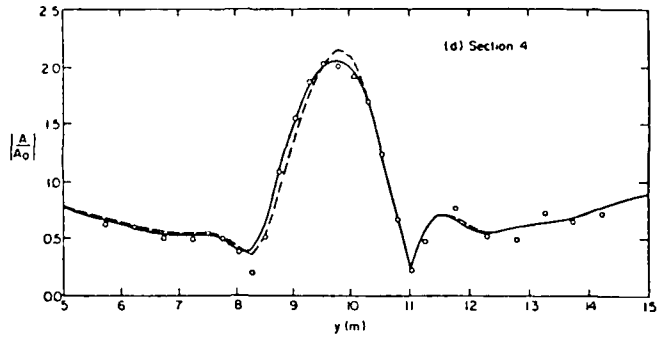

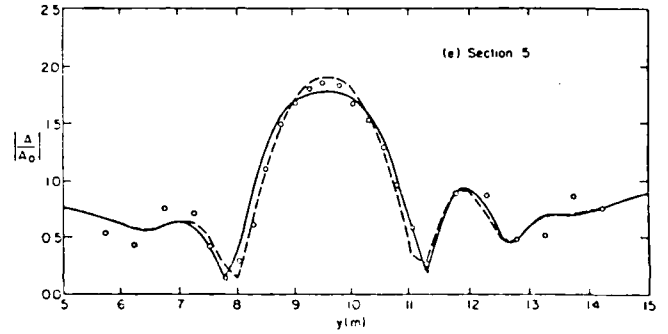

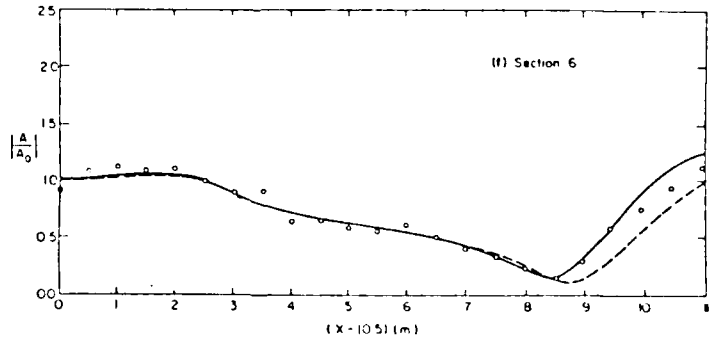

Figure 2.7.

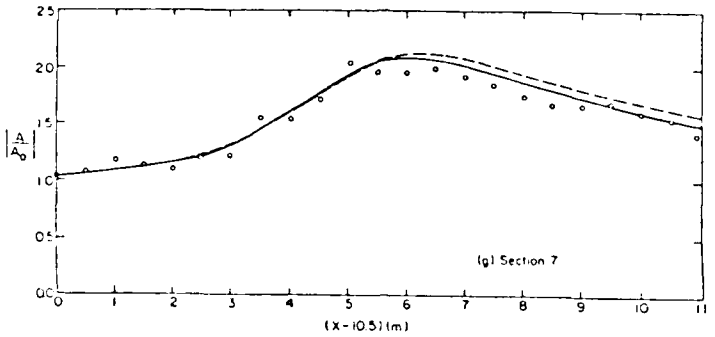

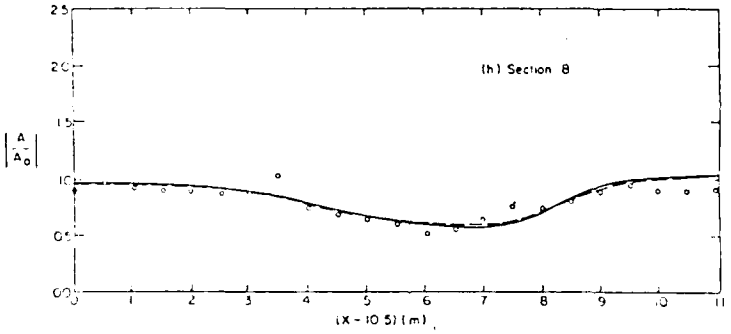

Figure 2.7. Comparison of model using the present composite dispersion relation (2.) to the Stokes model and laboratory data. ——— Stokes model; ----- composite model, o laboratory data. a-h) sections 1-8, respectively.

Secondly, although the difference between results of the Hedges and Stokes models is not severe, the errors in phase and group velocity would be expected to accumulate over long distances for waves propagating in shallow water. The proposed composite model reduces the small local error in the Hedges model by mixing the Hedges and Stokes effects together, and would be expected to produce more accurate results for waves propagating over large distances.

$$+ \frac{P_1 \beta_j^i}{\Delta y} \frac{(UV_j^{i+1} + UV_j^i)}{\sigma_{j-1}^i} + \left\{ \frac{i\Delta x}{4\Delta y^2} + \frac{2P_1}{(\Delta y)^2 (k_j^{i+1} + k_j^i)} - P_1 \beta_j^i \frac{\Delta x}{2\Delta y^2} \right\} \cdot$$

$$\cdot \frac{(PV_j^i + PV_{j-1}^i)}{\sigma_{j-1}^i} \tag{3.38}$$

and where

$$PV_j^i = (p - V^2)_j^i \tag{3.39}$$

$$\beta_j^i = \frac{4(k_j^{i+1} - k_j^i)}{(\Delta x)(k_j^{i+1} + k_j^i)^2} + \frac{8(k_j^{i+1}(p - U^2)_j^{i+1} - k_j^i (p - U^2)_j^i)}{(\Delta x)\left((k_j^{i+1} + k_j^i)\left((p - U^2)_j^{i+1} + (p - U^2)_j^i\right)\right)^2} \tag{3.40}$$

The remaining term C4 is given by

$$C4 = \frac{w}{2} A + \frac{i\sigma}{2} \left\{ \left(1 + f_1 (k|A|)^2 D\right) \frac{\tanh(kh + f_2 k|A|)}{\tanh kh} - 1 \right\} A \tag{3.41}$$

which is written out in finite difference form as

$$C4_j^i = \frac{1}{4} \{ w_j^{i+1} A_j^{i+1} + w_j^i A_j^i \}$$

$$+ \frac{i\sigma_j^{i+1}}{4} \left\{ \left(1 + f_{1_j}^{i+1} (k_j^{i+1})^2 |\tilde{A}_j^{i+1}|^2 D_j^{i+1}\right) \frac{\tanh(k_j^{i+1} h_j^{i+1} + f_{2_j}^{i+1} k_j^{i+1} |\tilde{A}_j^{i+1}|)}{\tanh(k_j^{i+1} h_j^{i+1})} - 1 \right\} A_j^{i+1}$$

$$+ \frac{i\sigma_j^i}{4} \left\{ \left(1 + f_{1_j}^i (k_j^i)^2 |A_j^i|^2 D_j^i\right) \frac{\tanh(k_j^i h_j^i + f_{2_j}^i k_j^i |A_j^i|)}{\tanh(k_j^i h_j^i)} - 1 \right\} A_j^i \tag{3.42}$$

$$C1_j^i = (C_g + U)_j^{i+1} + \left(1 - i\Delta x(\bar{k} - k)_j^i\right)(C_g + U)_j^i - \left(\frac{\sigma_j^{i+1} + \sigma_j^i}{4}\right)(\Delta V)_j^i$$

$$+ 2i\omega P_1 \beta_j^i (U_j^{i+1} + U_j^i) + \frac{4i\omega P_1}{(k_j^{i+1} + k_j^i)\sigma_j^i}\left\{\frac{3}{\Delta x}(U_j^{i+1} - U_j^i) + \frac{1}{4\Delta y}(V_{j+1}^{i+1} + V_{j+1}^i - V_{j-1}^{i+1} - V_{j-1}^i)\right.$$

$$+ \left\{-\frac{i\Delta x}{4\Delta y^2} - \frac{2P_1}{(k_j^{i+1} + k_j^i)\Delta y^2} + P_1\beta_j^i \frac{\Delta x}{2(\Delta y)^2}\right\} \frac{(PV_{j+1}^i + 2PV_j^i + PV_{j-1}^i}{\sigma_j^i} \qquad (3.36)$$

$$C2_j^i = -\frac{\Delta x}{4\Delta y}(V_j^{i+1} + V_j^i) + \frac{i}{4\Delta y}\frac{[UV_{j+1}^{i+1} + UV_{j+1}^i + 2UV_j^i]}{\sigma_{j+1}^i}$$

$$+ \frac{4iP_1\sigma_j^i V_j^i}{\Delta y(k_j^{i+1} + k_j^i)\sigma_{j+1}^i} - \frac{i}{2}\left(\frac{\Delta x}{\Delta y}\right) P_1\beta_j^i \frac{[\sigma V_j^{i+1} + \sigma V_j^i)}{\sigma_{j+1}^i}$$

$$+ \left\{-P_1\beta_j^i \frac{\Delta x}{2\Delta y^2} + \frac{2P_1}{(k_j^{i+1} + k_j^i)(\Delta y)^2} + \frac{i\Delta x}{4(\Delta y)^2}\right\} \frac{(PV_{j+1}^i + PV_j^i)}{\sigma_{j+1}^i}$$

$$- \frac{P_1\beta_j^i}{\Delta y} \frac{(UV_j^{i+1} + UV_j^i)}{\sigma_{j+1}^i} \qquad (3.37)$$

$$C3_j^i = \frac{\Delta x}{4\Delta y}(V_j^{i+1} + V_j^i) - \frac{i}{4\Delta y}\frac{[UV_{j-1}^{i+1} + UV_{j-1}^i + 2UV_j^i]}{\sigma_{j-1}^i}$$

$$- \frac{4iP_1\sigma_j^i V_j^i}{\Delta y(k_j^{i+1} + k_j^i)\sigma_{j-1}^i} + \frac{i}{2}\left(\frac{\Delta x}{\Delta y}\right) P_1\beta_j^i \frac{(\sigma V_j^{i+1} + \sigma V_j^i)}{\sigma_{j-1}^i}$$

$$CP2_j^i = \frac{\Delta x}{4\Delta y}\left(V_j^{i+1}+V_j^i\right) + \frac{i}{4\Delta y}\frac{\left[UV_{j+1}^{i+1} + UV_{j+1}^{i} + 2UV_j^{i+1}\right]}{\sigma_{j+1}^{i+1}}$$

$$+ \frac{4iP_1\sigma_j^{i+1}V_j^{i+1}}{\Delta y(k_j^{i+1} + k_j^i)\,\sigma_{j+1}^{i+1}} + \frac{i}{2}\left(\frac{\Delta x}{\Delta y}\right) P_1\beta_j^i \frac{(\sigma V_j^{i+1} + \sigma V_j^i}{\sigma_{j+1}^{i+1}}$$

$$- \frac{P_1\beta_j^i(UV_j^{i+1} + UV_j^i)}{\Delta y\,\sigma_{j+1}^{i+1}} + \left\{- \frac{i\Delta x}{4(\Delta y)^2} + \frac{2P_1}{(\Delta y)^2(k_j^{i+1} + k_j^i)} + \frac{P_1\beta_j^i\Delta x}{2(\Delta y)^2}\right\}$$

$$\cdot \frac{(PV_{j+1}^{i+1} + PV_j^{i+1})}{\sigma_{j+1}^{i+1}} \qquad (3.34)$$

$$CP3_j^i = - \frac{\Delta x}{4\Delta y}(V_j^{i+1} + V_j^i) - \frac{i}{4\Delta y}\frac{\left[UV_{j-1}^{i+1} + UV_{j-1}^{i} + 2UV_j^{i+1}\right]}{\sigma_{j-1}^{i+1}}$$

$$- \frac{4_iP_1\sigma_j^{i+1}V_j^{i+1}}{\Delta y(k_j^{i+1} + k_j^i)\sigma_{j-1}^{i+1}} - \frac{i}{2}\left(\frac{\Delta x}{\Delta y}\right) P_1\beta_j^i \frac{(\sigma V_j^{i+1} + \sigma V_j^i)}{\sigma_{j-1}^{i+1}}$$

$$+ \frac{P_1\beta_j^i(UV_j^{i+1} + UV_j^i)}{\Delta y\,(\sigma_{j-1}^{i+1})} + \left\{- \frac{i\Delta x}{4(\Delta y)^2} + \frac{2P_1}{(\Delta y)^2(k_j^{i+1} + k_j^i)} + \frac{P_1\beta_j^i\Delta x}{2(\Delta y)^2}\right\}$$

$$\cdot \frac{(PV_j^{i+1} + PV_{j-1}^{i+1})}{\sigma_{j-1}^{i+1}} \qquad (3.35)$$

$$A_j^i = A(i\Delta x,\ j\Delta y) \tag{3.30}$$

The computations proceed by updating values of A from the known "i" row to the unknown "i+1" row. Iterations for the nonlinear terms are performed using a repeated implicit calculation as in Kirby (1983).

Using the notation (3.30), (3.28) is written in finite difference form as

$$CP1_j^i\, A_j^{i+1} + CP2_j^i\, A_{j+1}^{i+1} + CP3_j^i\, A_{j-1}^{i+1}$$

$$= C1_j^i\, A_j^i + C2_j^i\, A_{j+1}^1 + C3_j^i\, A_{j-1}^i - 2(\Delta x)C4_j^i \tag{3.31}$$

where C1, C2, C3, CP1, CP2 and CP3 are known coefficients given by

$$CP1_j^i = (C_g + U)_j^{i+1}\{1 + i\Delta x(\bar{k} - k)_j^{i+1}\} + (C_g + U)_j^i + \left(\frac{\sigma_j^{i+1} + \sigma_j^i}{4}\right)(\Delta V)_j^i$$

$$+ 2i\omega P_1 \beta_j^i\,(\Gamma_j^{i+1} + \Gamma_j^i) + \frac{4i\omega P_1}{(k_j^{i+1} + k_j^i)\sigma_j^{i+1}}\left(\frac{3(U_j^{i+1} - U_j^i)}{\Delta x} + \frac{(V_{j+1}^{i+1} + V_{j+1}^i - V_{j-1}^{i+1} - V_{j-1}^i)}{4\Delta y}\right)$$

$$+ \left(\frac{i\bar{k}\Delta x}{4(\Delta y)^2} - \frac{2P_1}{(\Delta y)^2(k_j^{i+1} + k_j^i)} - P_1\beta_j^i\frac{\Delta x}{2(\Delta y)^2}\right)\frac{(PV_{j+1}^{i+1} + 2PV_j^{i+1} + PV_{j-1}^{i+1})}{\sigma_j^{i+1}} \tag{3.32}$$

where

$$(\Delta V)_j^i = \left(\frac{C_g + U}{\sigma}\right)_j^{i+1} - \left(\frac{C_g + U}{\sigma}\right)_j^i + \frac{\Delta x}{4\Delta y}\left[\left(\frac{V}{\sigma}\right)_{j+1}^{i+1} + \left(\frac{V}{\sigma}\right)_{j+1}^i - \left(\frac{V}{\sigma}\right)_{j-1}^{i+1} - \left(\frac{V}{\sigma}\right)_{j-1}^i\right]$$

(3.33)

$$(C_g + U)A_x + VA_y + i(\bar{k} - k)(C_g + U)A + \frac{\sigma}{2}\left\{\left(\frac{C_g + U}{\sigma}\right)_x + \left(\frac{V}{\sigma}\right)_y\right\}A$$

$$- \frac{i}{2}\left[(p - V^2)\left(\frac{A}{\sigma}\right)_y\right]_y + \frac{i}{2}\left\{\left(UV\left(\frac{A}{\sigma}\right)_y\right)_x + \left(UV\left(\frac{A}{\sigma}\right)_x\right)_y\right\} + \frac{i\sigma}{2} k^2 D|A|^2 A$$

$$+ \frac{w}{2} A + \frac{P_1}{k}\left\{\left[(p - V^2)\left(\frac{A}{\sigma}\right)_y\right]_{yx} + 2i\left(\sigma V\left(\frac{A}{\sigma}\right)_y\right)_x\right\}$$

$$+ P_1 3\left\{2i\omega U\left(\frac{A}{\sigma}\right)_x + 2i\sigma V\left(\frac{A}{\sigma}\right)_y - 2UV\left(\frac{A}{\sigma}\right)_{xy} + \left[(p - V^2)\left(\frac{A}{\sigma}\right)_y\right]_y\right\}$$

$$+ \frac{i}{k} P_1\left\{(\omega V)_y + 3(\omega U)_x\right\}\left(\frac{A}{\sigma}\right)_x = 0 \qquad (3.28)$$

This equation extends the published results in Kirby (1984) and Kirby and Dalrymple (1983b) to the case of waves propagating at large angles to the x-direction in the presence of a current. Nonlinearity here is consistent with the lowest order Stokes formulation of Kirby and Dalrymple (1983a). The nonlinear term may be directly modified according to the results in Chapter 2. The resulting equation is of the form

$$(C_g + U)A_x + \frac{i\sigma}{2}\left\{(1 + f_1(k|A|)^2 D \frac{\tanh(kh + f_2 k|A|)}{\tanh kh} - 1\right\}A + \ldots = 0 \quad (3.29)$$

where f_1, f_2 and D are functions of kh given by (2.36), (2.37), and (2.3) respectively.

3.2 Finite Difference Scheme

The finite difference scheme for (3.28) follows directly using the Crank-Nicolson method for performing an implicit update for each row in x. The notation of Kirby (1983), section 6.2 is retained. We denote x-positions by "i" superscripts and y-positions by "j" subscripts. For example:

where α_1' and α_3' are α_1 and α_3 written in terms of A. The first bracketed term is given by

$$\{\beta\alpha_1' + \beta(R_1\tilde{\phi})e^{-i\bar{\psi}} + \frac{i}{k}\alpha_3'\}$$

$$= \beta\{2i\omega U(\frac{A}{\sigma})_x + i(\omega U)_x(\frac{A}{\sigma}) - 2\omega Uk(\varepsilon - 1)(\frac{A}{\sigma})$$

$$+ 2i\sigma V(\frac{A}{\sigma})_y + i(\sigma V)_y(\frac{A}{\sigma}) - i(k(\varepsilon - 1)UV)_y(\frac{A}{\sigma})$$

$$- 2ik(\varepsilon - 1)UV(\frac{A}{\sigma})_y - (UV(\frac{A}{\sigma})_x)_y - (UV(\frac{A}{\sigma})_y)_x$$

$$+ [(p - V^2)(\frac{A}{\sigma})_y]_y\}$$

$$+ \frac{i}{k}\{(\omega V)_{xy}(\frac{A}{\sigma}) + (\omega U)_{xx}(\frac{A}{\sigma}) + (\omega V)_y(\frac{A}{\sigma})_x + ik(\varepsilon - 1)(\omega V)_y(\frac{A}{\sigma})$$

$$+ 3(\omega U)_x(\frac{A}{\sigma})_x + 3ik(\varepsilon - 1)(\omega U)_x\frac{A}{\sigma}\} \qquad (3.27)$$

So far, nothing has been dropped besides some second derivatives of currents. In order to simplify the equation further, we drop the following terms as being small:

1) Terms in $(1 - \varepsilon)$ multiplying products of current components or derivatives.
2) Terms with β multiplying derivatives of the ambient current.

We are then left with the form of the equation to be used in the numerical scheme.

$$P_2 - P_1(\bar{k}/k) = P_2 - P_1 + P_1(1 - \bar{k}/k)$$

$$= \frac{1}{2} + P_1\left(1 - \frac{\bar{k}}{k}\right) \tag{3.25}$$

Denote $\varepsilon \equiv \bar{k}/k$. It is usually assumed that $\varepsilon \simeq 1$; i.e., the wave number varies only slightly along a grid row. Making this assumption, we may take $1 - \varepsilon \ll O(1)$, introducing a small parameter. The full equation for A defined according to

$$\tilde{\phi} \equiv -\frac{ig}{2}\left(\frac{A}{\sigma}\right) e^{i\bar{\psi}} + c.c.$$

is given by

$$(C_g + U)A_x + VA_y + i(\bar{k} - k)(C_g + U)A + \frac{\sigma}{2}\left\{\left(\frac{C_g + U}{\sigma}\right)_x + \left(\frac{V}{\sigma}\right)_y\right\}A$$

$$+ \frac{i}{2}\sigma k^2 D|A|^2 A + \frac{w}{2}A - \frac{i}{2}\left[(p - V^2)\left(\frac{A}{\sigma}\right)_y\right]_y$$

$$+ \frac{i}{2}\left\{\left(UV\left(\frac{A}{\sigma}\right)_x\right)_y + \left(UV\left(\frac{A}{\sigma}\right)_y\right)_x\right\}$$

$$+ \frac{P_1}{k}\left\{\left[(p - V^2)\left(\frac{A}{\sigma}\right)_y\right]_{yx} + 2i\left[\sigma V\left(\frac{A}{\sigma}\right)_y\right]_x\right\}$$

$$+ P_1\left\{\beta\alpha_1' + \beta R_1 e^{-i\bar{\psi}} + \frac{i}{k}\alpha_3'\right\}$$

$$+ (\varepsilon - 1)kUV\left(\frac{A}{\sigma}\right)_y - \frac{1}{2}\left\{(\varepsilon - 1)kUV\right\}_y\left(\frac{A}{\sigma}\right) + \frac{P_1}{k}\left\{2i\left[(1 - \varepsilon)kUV\left(\frac{A}{\sigma}\right)_y\right]_x\right.$$

$$\left. - k(1 - \varepsilon)(\varepsilon kUV)_y\left(\frac{A}{\sigma}\right) + 2k(1 - \varepsilon)\sigma V\left(\frac{A}{\sigma}\right)_y - ik(1 - \varepsilon)(p - V^2)\left(\frac{A}{\sigma}\right)_y\right]_y$$

$$+ ik(1 - \varepsilon)\left\{\left[UV\left(\frac{A}{\sigma}\right)_y\right]_x + \left[UV\left(\frac{A}{\sigma}\right)_x\right]_y\right\} = 0 \tag{3.26}$$

The right-hand side of (3.17) becomes

$$\text{R.H.S.} = (\omega U)\left(\frac{A'}{\sigma}\right)_x + \frac{1}{2}(\omega U)_x\left(\frac{A'}{\sigma}\right) + iP_2\alpha_1 + iP_2R_1(\tilde{\phi})e^{-i\psi}$$

$$- \frac{P_1}{k}\alpha_2 - \frac{P_1}{k}R_2(\tilde{\phi})e^{-i\psi} + P_1\beta\alpha_1 + P_1\beta R_1(\tilde{\phi})e^{-i\psi} \qquad (3.21)$$

Evaluating $iP_2\alpha_1 - (P_1/k)\alpha_2$ gives

$$iP_2\alpha_1 - \left(\frac{P_1}{k}\right)\alpha_2 = -(\omega U)\left(\frac{A'}{\sigma}\right)_x - \left(\frac{\omega U}{2}\right)_x\left(\frac{A'}{\sigma}\right) - \left(\frac{\omega V}{2}\right)_y\left(\frac{A'}{\sigma}\right) - i\frac{P_1}{k}\alpha_3 \qquad (3.22)$$

where

$$\alpha_3 = (\omega V)_{xy}\left(\frac{A'}{\sigma}\right) + (\omega U)_{xx}\left(\frac{A'}{\sigma}\right) + (\omega V)_y\left(\frac{A'}{\sigma}\right)_x + 3(\omega U)_x\left(\frac{A'}{\sigma}\right)_x \qquad (3.23)$$

The R.H.S. of (3.17) reduces to

$$\text{R.H.S.} = -\frac{1}{2}(\sigma V)_y\left(\frac{A'}{\sigma}\right) - \frac{1}{2}(kUV)_y\left(\frac{A'}{\sigma}\right) - i\frac{P_1}{k}\alpha_3$$

$$+ \left[iP_2(R_1\tilde{\phi}) - \frac{P_1}{k}(R_2\tilde{\phi})\right]e^{-i\psi} + P_1\beta(\alpha_1 + R_1(\tilde{\phi})\,e^{-i\psi}) \qquad (3.24)$$

We now need to simplify R_1 and R_2. Shifting to the reference phase $\bar{\psi}$ defined in (3.6), we continue to expand all terms in order to eliminate the phase function ψ and $\bar{\psi}$. The use of $\bar{\psi}$ injects a $\bar{k}$ in the equation in place of k in some terms. Note that

will have some contributions like

$$iP_2(M\tilde{\phi}) - \frac{P_1}{k} M(\tilde{\phi}_x) \approx i(P_2 - P_1)\,(M\tilde{\phi}) \sim \frac{i}{2}\,(M\tilde{\phi})$$

These will balance the { } terms above in (3.16) and give the lowest order diffraction and y-direction transport terms. Terms without y derivatives may be manipulated simply. In terms of the complex amplitude A', $M\tilde{\phi}$ becomes

$$\begin{aligned}(M\tilde{\phi})e^{-i\psi} &= i(\omega U)_x\left(\frac{A'}{\sigma}\right) + i(\omega V)_y\left(\frac{A'}{\sigma}\right) + 2i\omega U\left(\frac{A'}{\sigma}\right)_x \\ &\quad + \left\{2i\omega V\tilde{\phi}_y + \left[(p - V^2)\,\tilde{\phi}_y\right]_y - (UV\tilde{\phi}_x)_y - (UV\tilde{\phi}_y)_x e^{-i\psi}\right. \\ &= \alpha_1 + (R_1\tilde{\phi})\,e^{-i\psi} \qquad (3.19)\end{aligned}$$

where the phase is successfully eliminated from α_1. Differentiating (3.19) gives

$$\begin{aligned}(M\tilde{\phi})_x e^{-i\psi} &= \left\{-k(\omega U)_x\left(\frac{A'}{\sigma}\right) - 2k\omega U\left(\frac{A'}{\sigma}\right)_x + i(\omega V)_{xy}\left(\frac{A'}{\sigma}\right)\right. \\ &\quad + i(\omega V)_y\left(\frac{A'}{\sigma}\right)_x - k(\omega V)_y\left(\frac{A'}{\sigma}\right) + i(\omega U)_{xx}\left(\frac{A'}{\sigma}\right) \\ &\quad \left. + 3i(\omega U)_x\left(\frac{A'}{\sigma}\right)_x\right\} \\ &\quad + \left\{2i(\omega V)_x\tilde{\phi}_y + 2i(\omega V)\tilde{\phi}_{xy} + \left[(p - V^2)\tilde{\phi}_y\right]_{xy}\right. \\ &\quad \left. - (UV\tilde{\phi}_x)_{xy} - (UV\tilde{\phi}_y)_{xx}\right\} e^{-i\psi} \\ &= \alpha_2 + (R_2\tilde{\phi})\,e^{-i\psi} \qquad (3.20)\end{aligned}$$

(3.13) is then given by

$$\sigma(C_g + U)\,\tilde{\phi}_x + \frac{1}{2}\left[\sigma(C_g + U)\right]_x\tilde{\phi} - ik\sigma(C_g + U)\,\tilde{\phi}$$

$$+ \frac{i}{2}\,\sigma^2k^2D|A'|^2\,\tilde{\phi} + \sigma\,\frac{w}{2}\,\tilde{\phi}$$

$$- \{\omega U\tilde{\phi}_x + \frac{1}{2}\,(\omega U)_x\tilde{\phi} - ik\omega U\tilde{\phi}\} - iP_2M\tilde{\phi}$$

$$+ \frac{P_1}{k}\,(M\tilde{\phi})_x - P_1\beta M\tilde{\phi} \;=\; 0 \qquad (3.16)$$

The term $\{\ \}$ will be cancelled by leading order contributions from $P_2M\tilde{\phi}$. Substituting for $\tilde{\phi}$ using (3.11) gives

$$(C_g + u)A'_x + \frac{\sigma}{2}\left(\frac{C_g + U}{\sigma}\right)_xA' + \frac{i}{2}\,\sigma k^2D|A'|^2A' + \frac{w}{2}\,A'$$

$$= \omega U\left(\frac{A'}{\sigma}\right)_x + \frac{1}{2}\,(\omega U)_x\left(\frac{A'}{\sigma}\right) + iP_2M\tilde{\phi}e^{-i\psi} - \frac{P_1}{k}(M\tilde{\phi})_xe^{-i\psi}$$

$$+ P_1\beta(M\tilde{\phi})e^{-i\psi} \qquad (3.17)$$

The right-hand side remains to be simplified. Note that

$$\tilde{\phi}_y \;=\; \left[\left(\frac{A'}{\sigma}\right)_y + i\psi_y\left(\frac{A'}{\sigma}\right)\right]e^{i\psi} \qquad (3.18)$$

Also, terms in

$$iP_2(M\tilde{\phi}) - \frac{P_1}{k}\,(M\tilde{\phi})_x$$

We will use a local phase and amplitude according to

$$\tilde{\phi} = -ig\left(\frac{A'}{\sigma}\right)e^{i\psi}; \quad \psi = \int k(x,y)dx - \omega t \tag{3.11}$$

So that

$$\frac{\partial\tilde{\phi}}{\partial x} = -ig\left[\left(\frac{A'}{\sigma}\right)_x + ik\left(\frac{A'}{\sigma}\right)\right]e^{i\psi} \simeq ik\tilde{\phi} \text{ at lowest order}$$

Expanding (3.8) and multiplying by $\gamma^{1/2}$ gives

$$\frac{i}{2}\frac{\partial\gamma}{\partial x}\tilde{\phi} + \gamma\frac{\partial\tilde{\phi}}{\partial x} - P_1\left(\frac{\partial k}{\partial x}/k^2\right)M\tilde{\phi} - P_1\left(\frac{\partial\gamma}{\partial x}/2k\gamma\right)M\tilde{\phi}$$

$$+ \frac{P_1}{k}\left(M\tilde{\phi}\right)_x - iP_2M\tilde{\phi} - ik\gamma\tilde{\phi} - i(P_2 - P_1)N\tilde{\phi} \tag{3.12}$$

Note that $P_2 - P_1 = 1/2$ whatever the value of P_1; so that

$$\gamma\frac{\partial\tilde{\phi}}{\partial x} + \frac{1}{2}\frac{\partial\gamma}{\partial x}\tilde{\phi} - ik\gamma\tilde{\phi} - \frac{i}{2}N\tilde{\phi} + \frac{P_1}{k}\left(M\tilde{\phi}\right)_x - iP_2\left(M\tilde{\phi}\right)$$

$$- P_1\left\{\frac{\frac{\partial k}{\partial x}}{k^2} + \frac{\frac{\partial}{\partial x}\left(k(p - U^2)\right)}{2k^2(p - U^2)}\right\}\left(M\tilde{\phi}\right) = 0 \tag{3.13}$$

Define:

$$\beta \equiv \frac{k_x}{k^2} + \frac{\left(k(p - U^2)\right)_x}{2k^2(p - U^2)} \tag{3.14}$$

And note that

$$\gamma = kp - kUU = \sigma(C_g + U) - \omega U \tag{3.15}$$

$$(UV)_{xy}A,\ (UV)_xA_y,\ UV\,A_{xy}$$

will be dropped.

Finally, a reference phase function is defined according to

$$\bar{\psi} = \int_x \bar{k}(x)dx - \omega t \tag{3.6}$$

where

$$\bar{k}(x) = \int_{y_1}^{y_2} k(x,y)dy \Big/ \int_{y_1}^{y_2} dy \tag{3.7}$$

is the average of the linear wave number over a y-coordinate grid row. We now proceed by reducing (3.1) to a usable form.

Denote $k(p - U^2) = \gamma$. Then, (3.1) may be written as

$$\frac{\partial}{\partial x}\left(\gamma^{1/2}\phi\right) + \frac{\partial}{\partial x}\left(k^{-1}\gamma^{-1/2}P_1M'\phi\right)$$

$$= ik\gamma^{1/2}\phi + i\gamma^{-1/2}P_2\left(M'\phi\right) \tag{3.8}$$

Denote $M'\tilde{\phi} = M\tilde{\phi} + N\tilde{\phi}$, where N are the localized nonlinear and dissipation terms. Then

$$\left(M\tilde{\phi}\right) = \left(2\omega kU + i\omega\nabla\cdot\underline{U}\right)\tilde{\phi} + 2i\omega\underline{U}\cdot\nabla\tilde{\phi} + \left((p - V^2)\tilde{\phi}_{..}\right)$$

$$- \left(UV\tilde{\phi}_x\right)_y - \left(UV\tilde{\phi}_y\right)_x \tag{3.9}$$

$$N\tilde{\phi} = -\sigma^2k^2D|A|^2\,\tilde{\phi} + i\sigma w\tilde{\phi} \tag{3.10}$$

gradient operator, and w represents a damping coefficient due to the presence of boundary layers or porous bottom damping (Dalrymple et al, 1984) or wave breaking (Kirby, 1983). Kirby (1983) developed (3.1) with $\underset{\sim}{U} \equiv 0$, and $P_1 = 1/4$ in its full form and gave the numerical scheme for the large angle approximation without currents. This chapter provides the same information for the case of waves interacting with a pre-specified ambient current. Section 3.1 gives the derivation of an evolution equation for complex amplitude A based on (3.1) with $P_1 = 1/4$. Section 3.2 provides the finite difference form of the evolution equation using the Crank-Nicolson approximation.

3.1. The Parabolic Equation for Waves on Currents

As a first step, the parabolic equation for $\tilde{\phi}$ is developed. Several simplifying assumptions will be employed. First, nonlinear terms and dissipative terms will be considered to be grouped with the highest order contributions in the equation, and only the largest contributions resulting from manipulations to these terms will be retained. For example:

$$\frac{\partial}{\partial x}\left(\sigma^2 k^2 D|A|^2 \tilde{\phi}\right) \approx \sigma^2 k^2 D|A|^2 \frac{\partial \tilde{\phi}}{\partial x} \approx i\sigma^2 k^3 D|A|^2 \tilde{\phi} \qquad (3.5)$$

These terms will therefore not retain any derivatives related to the slow spatial scale of variation.

Booij (1981) drops all terms containing products of ambient velocity components. Here, these terms will be retained up to the level of second derivatives; i.e., terms such as

Chapter 3. Large Angle Formulation for the Wave-Current Model

Kirby (1983) provided a higher-order, large angle formulation of the parabolic approximation for waves on currents, following the original work of Booij (1981). The governing equation for the value of the velocity potential $\tilde{\phi}$ at the mean water level is given by Kirby (1983) as

$$\left\{k(p - U^2)^{1/2} \left(1 + \frac{P_1 M'}{k^2(p - U^2)}\right) \tilde{\phi}\right\}_x = ik\left[k(p - U^2)\right]^{1/2} \left(1 + \frac{P_2 M'}{k^2(p - U^2)}\right) \tilde{\phi} \tag{3.1}$$

where

$$p = CC_g \tag{3.2}$$

$$P_1 = P_2 - 1/2 = 0 \text{ or } 1/4 \tag{3.3}$$

and

$$\begin{aligned} M' \tilde{\phi} = {} & \left(2\omega kU + i\omega \nabla_h \cdot \underset{\sim}{U}\right) \tilde{\phi} + 2i\omega \underset{\sim}{U} \cdot \nabla_h \tilde{\phi} \\ & - (UV\tilde{\phi}_x)_y - (UV\tilde{\phi}_y)_x + \left[(p - V^2)\tilde{\phi}_y\right]_y \\ & - \sigma^2 k^2 D|A|^2 \tilde{\phi} + i\sigma w \tilde{\phi} \end{aligned} \tag{3.4}$$

The choice $P_1 = 0$ reduces the model to the lowest order approximation of Radder (1979) or Kirby (1983,1984). The choice $P_1 = 1/4$ gives the higher order approximation proposed by Booij (1981). Finally, $\underset{\sim}{U} = (U,V)$ represents the ambient current in x and y coordinates, ∇_h represents the horizontal

Here, the unknown $\tilde{A}_j^{i+1}$ is given by the last updated value of A_j^{i+1} in the iteration procedure. Chapter 4 describes how wave breaking is incorporated in the specification of the dissipation coefficient w.

Chapter 4. Modelling Waves in Surfzones and Around Islands

4.1. Introduction

In recent years, the parabolic equation method for wave propagation has seen a rapid development in the context of predicting surface water waves over areas of variable bathymetry, including both the effects of refraction and diffraction. The original development of the model was based either on a splitting of the elliptic mild slope equation of Berkhoff (1972) into coupled equations for forward- and back-scattered wave motion, as in Radder (1979), or on direct perturbation expansion of the governing equations using the WKB formalism, as in Liu and Mei (1976). Recent extensions of the capabilities of the parabolic method include the modelling of wave-current interaction (Booij (1981), Kirby (1984)), iterative calculation of the reflected wave field (Liu and Tsay (1983)), and the inclusion of lowest order nonlinear effects in the Stokes wave formulation (Kirby and Dalrymple (1983, 1984), Liu and Tsay (1984)).

An advantage of the parabolic method over solution techniques for elliptic and hyperbolic equations is that no downwave boundary condition is needed for the solution of the initial boundary value problem. However, in applications of wave models to coastal areas, accurate modelling of the behavior of waves in the vicinity of a physical downwave boundary consisting of an actual coastline or an offshore island is of primary importance to the prediction of known physical effects such as wave-induced runup, longshore currents and scour.

Wave breaking in the surf zone is a complex, highly nonlinear phenomenon. It is obvious that the parabolic equation method, which is limited to the representation of linear or weakly nonlinear wave fields, is

basically incapable at present of representing the underlying physics of the breaking process. However, some progress can be made by shifting our view of the model from its physical basis to its use as a predictive tool.

The forces leading to the generation and maintenance of setup and wave-induced currents depend on a physical balance between gradients of excess momentum fluxes, pressure forces due to changes in mean surface elevation, and bottom shear stresses. The role of a wave model in determining the balance consists of predicting the local wave energy density and direction of propagation of the wave field. Thus, as a lowest approximation of the overall physics, it suffices that the wave model be able to predict the local wave amplitude in the breaking zone with some degree of reliability.

The simplest model of wave decay in the surf zone, the spilling breaker model, is based on the assumption that the ratio of wave height to local water depth has the same value everywhere in the surf zone as at the breaker line. This assumption has been used extensively in the literature, from predictions of setup (Longuet-Higgins and Stewart (1963)) and longshore currents (Longuet-Higgins (1970)) up to the latest applications of numerical refraction schemes to the study of wave-induced circulation over arbitrary bottoms (e.g., Ebersole and Dalrymple (1980)). However, it has long been known that breaking waves, especially of the plunging type, do not follow so simple a rule. Extensive model tests of normally incident wave trains breaking on laboratory beaches have shown that the pattern of wave height decay across the surf zone is strongly a function of the beach slope. Representative measurements of Horikawa and Kuo (1966) are shown for example in Figure 4.1 in comparison to their dissipation model.

The purpose of the present study is to relate an empirical model of surf zone wave energy decay to the dissipation coefficient w of the dissipative

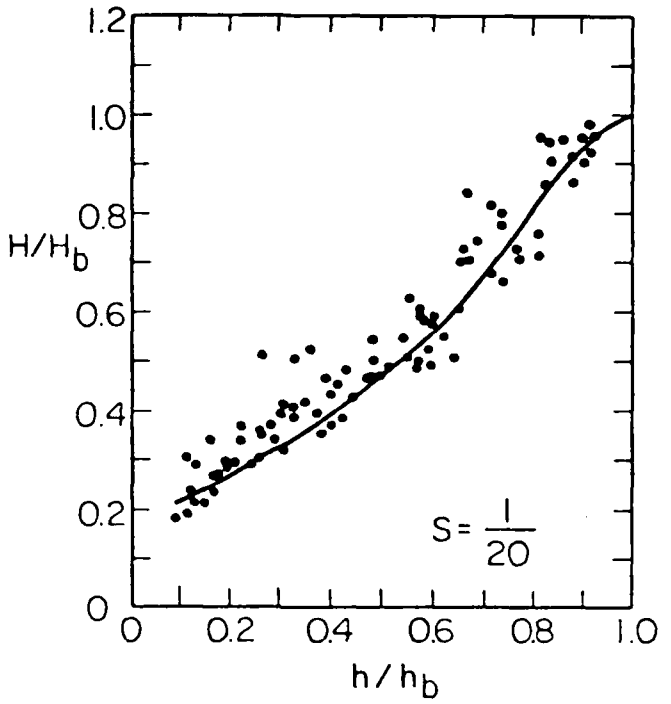

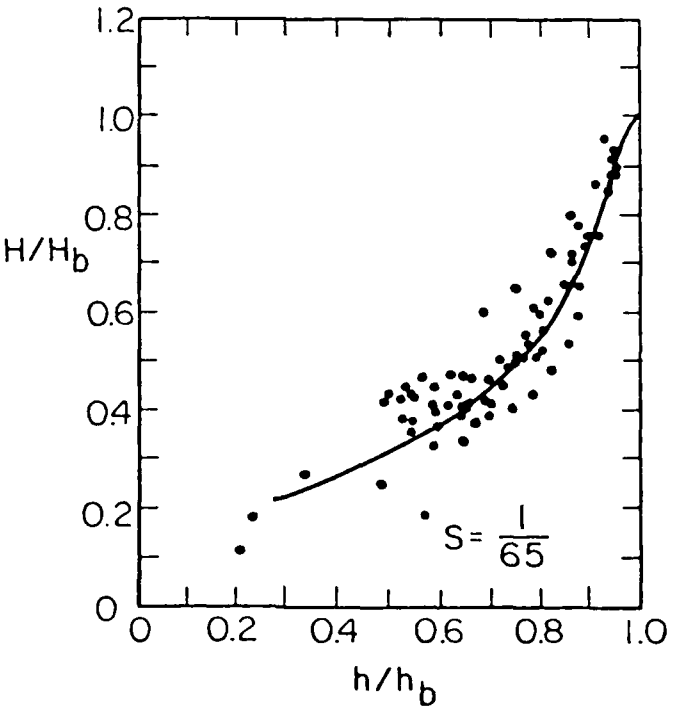

Figure 4.1. Measured wave heights in a laboratory surfzone a) beach slope s = 1:20, b) s = 1:65 (from Horikawa and Kuo, 1966).

wave model of Dalrymple, Kirby and Hwang (1984), and to detail the application of the model to the prediction of wave height in the surf zone. Here, the model of Dally, Dean and Dalrymple (1984) is used, although any of the related models for dissipation in bores could be applied just as well (Horikawa and Kuo, 1966; Divoky et al, 1970; Battjes and Janssen, 1978, for example).

4.2. The Energy Decay Model

Dally, Dean and Dalrymple (1984) have proposed that the decay of energy flux with distance in the surf zone is proportional to the excess of energy flux over a stable value, given for waves propagating shoreward in the x direction by the relation

$$\frac{\partial}{\partial x}(EC_g) = -\frac{K}{h}\left(EC_g - (EC_g)_s\right) \qquad (4.1)$$

where h is the local water depth and K is a constant to be determined, which is related to the rate of energy decay. The quantity $(EC_g)_s$ is the "stable" energy flux for a broken wave in water of depth h. Here E is $1/8\ \rho g H^2$, H is the local wave height and $C_g = \left(1 + \frac{2kh}{\sinh 2kh}\right)/2$ where ρ is the fluid density, g is the acceleration of gravity and k and h are related by the dispersion relationship, $\omega^2 = gk \tanh kh$. Here $\omega = 2\pi/T$, where T is the wave period. Dally et al. show that this model of wave energy decay is analogous to the energy loss in a hydraulic jump. The stable energy flux may be related to the height obtained asymptotically by a wave propagating over a flat bottom or a plane slope. Measurements by Horikawa and Kuo (1966) indicate that a value of $H_s = 0.4\ h$ is approached for waves breaking on a plane slope. In the following derivation, we denote $(H/h)_s = \gamma$, where γ is an empirical constant.

Equation (4.1) may be related to a wave energy equation for dissipative motion after assuming a time-steady wave field. For normally incident waves, the energy equation becomes

$$\frac{\partial}{\partial x}(EC_g) = -WE \tag{4.2}$$

Noting that $C_{gs} = C_g$, W may be written as

$$W = \frac{KC_g}{h}\left(1 - \frac{E_s}{E}\right) = \frac{KC_g}{h}\left(1 - \frac{H_s^2}{H^2}\right) \tag{4.3}$$

where $H = 2|A|$, and A is a generally complex measure of wave amplitude and phase.

For a plane beach with slope s, and neglecting the effect of setup (which is not calculated by the wave model directly), a simple analytic solution of (4.1) was obtained by Dally et al. Their comparison to laboratory data of breaking waves shows that this model very successfully represents wave height decay across the surf zone. This analytical model will therefore be used for comparison with the numerical model. Defining $\alpha = K/s$, the wave height in dimensionless form is related to the local water depth by:

$$\left(\frac{H}{H_b}\right)^2 = \left(\frac{h}{h_b}\right)^2 \left[(1-\Delta)\left(\frac{h}{h_b}\right)^{\alpha-5/2} + \Delta\right] \quad ; \quad \alpha \neq \frac{5}{2} \tag{4.4}$$

where

$$\Delta = \frac{\alpha}{\alpha-5/2}\left(\frac{\gamma}{\kappa}\right)^2 \quad ; \quad \kappa = \frac{H_b}{h_b} \text{ (at breaking)} \tag{4.5}$$

and

$$\left(\frac{H}{H_b}\right)^2 = \left(\frac{h}{h_b}\right)^2 \left[1 - \frac{5}{2}\left(\frac{\gamma}{\kappa}\right)^2 \ell n\left(\frac{h}{h_b}\right)\right] \quad ; \quad \alpha = \frac{5}{2} \cdot \tag{4.6}$$

Based on comparisons to the laboratory data of Horikawa and Kuo (1966), Dally et al. chose the value $K = 0.15$. The special case $\alpha = 5/2$ then corresponds to a beach slope $s = 0.06$. Results for a range of α values of $1 < \alpha < 10$, corresponding to the range of beach slopes $0.15 > s > 0.015$, are given in Figure 4.2 for $\gamma = 0.4$, $\kappa = 0.78$. The lines labelled 1 and 2 correspond to the constant decay $H = \kappa h = 0.78\ h$ and to the stable wave height $H_s = \gamma h = 0.4\ h$, respectively. The effect of beach slope, s, is clearly apparent. For mild slopes, α is large and the wave heights across the surf zone are much less than given by the spilling breaker model, while, for steep beaches, α is small and the wave heights exceed the spilling breaker model ($H = \kappa h$) heights. The paper by Dally et al. contains an extensive comparison between these results and the data of Horikawa and Kuo (1966).

4.3. Application of the Model in the Parabolic Equation Method

The results (4.4-6) provide a check for determining the accuracy of iterative schemes using the wave damping term (4.3). Noting that $H_s = \gamma h$ and $H = 2|A|$, (4.3) may be written as

$$W = \frac{KC_g}{h}\left(1 - \frac{\gamma^2 h^2}{4|A|^2}\right) \cdot \tag{4.7}$$

Assuming that the reflected wave (in the minus x direction) is small, we use the parabolic equation given by (3.28) to obtain

$$A_x - i(k-k_o)A + \frac{1}{2C_g} C_{gx} A - \frac{i}{2C_g\omega} (CC_g A_y)_y + wA = 0 \tag{4.8}$$

where we have neglected currents and nonlinear effects.

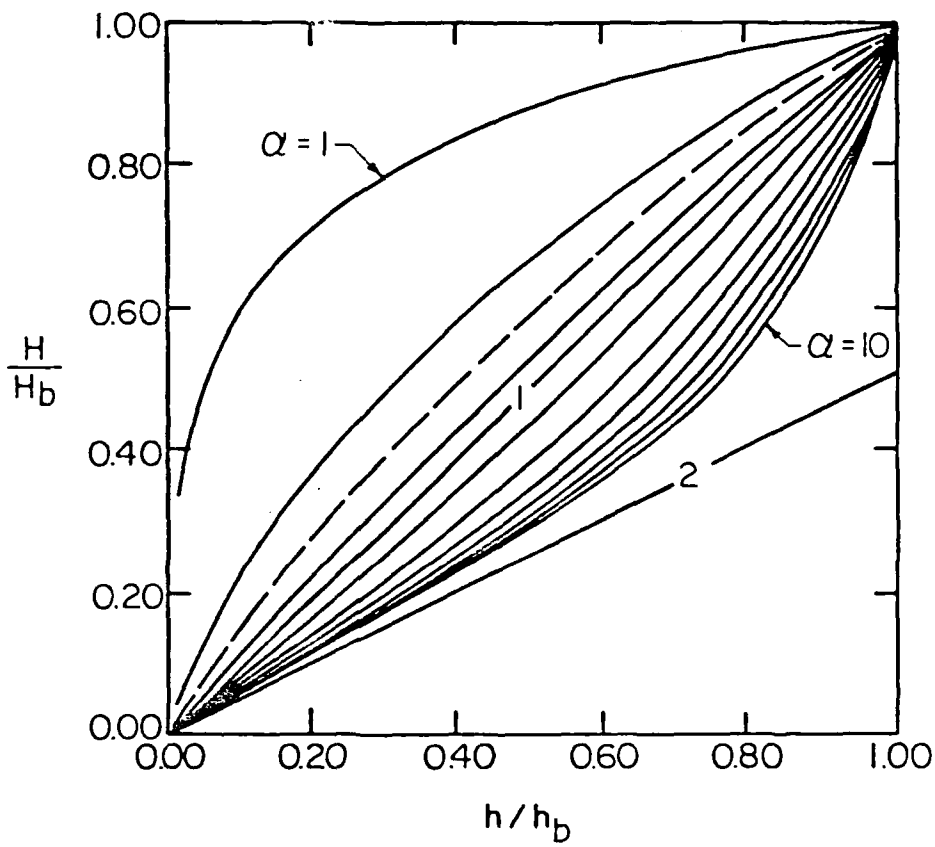

Figure 4.2. Surfzone wave height, plane beach. ——— α = 1-10; ----- α = 5/2. 1. Constant height/ depth, H = kh. 2. H = γ h.

Subscripts x and y denote differentiation. Here, A(x,y) is the complex amplitude of a steady wave train

$$\eta(x,y,t) = \mathrm{Re}\left\{ A(x,y)\, e^{i(k_o x - \omega t)} \right\} , \tag{4.9}$$

k_o is a reference value of the wavenumber based on a constant water depth which is characteristic of the domain, and

$$w = \frac{W}{2C_g} = \frac{K}{2h}\left(1 - \frac{\gamma^2 h^2}{4|A|^2}\right) \quad . \tag{4.10}$$

Here we choose a real value of w in contrast to the results for boundary layer damping (Liu, 1984), since the wave breaking process would not be expected to distort the wavelength in the same manner as a small dissipation due to viscous effects. Equation (4.8) is written in finite difference form according to the Crank-Nicolson method:

$$\frac{A_j^{i+1} - A_j^i}{\Delta x} - \frac{i}{2}\left[\left(k_j^{i+1} - k_o\right) A_j^{i+1} + \left(k_j^i - k_o\right) A_j^i\right]$$

$$+ \frac{C_{g_j}^{i+1} - C_{g_j}^{i}}{4\Delta x}\left[\frac{A_j^{i+1}}{C_{g_j}^{i+1}} + \frac{A_j^i}{C_{g_j}^i}\right] - \frac{i}{4\omega}\left\{\frac{(CC_g A_y)_{y_j}^{i+1}}{C_{g_j}^{i+1}} + \frac{(CC_g A_y)_{y_j}^{i}}{C_{g_j}^{i}}\right\}$$

$$+ \frac{1}{2}\left(w_j^{i+1} A_j^{i+1} + w_j^i A_j^i\right) = 0 \tag{4.11}$$

where y-derivative terms are given by

$$(CC_g A_y)_{y_j}^{i} = \frac{(CC_{g_{j+1}}^{i} + CC_{g_j}^{i})(A_{j+1}^{i} - A_j^{i}) - (CC_{g_j}^{i} + CC_{g_{j-1}}^{i})(A_j^{i} - A_{j-1}^{i})}{2(\Delta y)^2} \tag{4.12}$$

and where

$$w_j^{i+1} = \frac{K}{2h_j^{i+1}}\left[1 - \frac{\gamma^2 (h_j^{i+1})^2}{4|\tilde{A}_j^{i+1}|^2}\right] \tag{4.13}$$

The intermediate value $\tilde{A}_j^{i+1}$ is provided by information on the starting grid row according to

$$\frac{\tilde{A}_j^{i+1} - A_j^{i}}{\Delta x} - \frac{i}{2}\left[(k_j^{i+1} - k_o)\tilde{A}_j^{i+1} + (k_j^{i} - k_o)A_j^{i}\right]$$

$$+ \frac{(C_{g_j}^{i+1} - C_{g_j}^{i})}{4\Delta x}\left[\frac{\tilde{A}_j^{i+1}}{C_{g_j}^{i+1}} + \frac{A_j^{i}}{C_{g_j}^{i}}\right] - \frac{i}{4\omega}\left[\frac{(CC_g \tilde{A}_y)_{y_j}^{i+1}}{C_{g_j}^{i+1}} + \frac{(CC_g A_y)_{y_j}^{i}}{C_{g_j}^{i}}\right]$$

$$+ \frac{1}{2}\left(\tilde{w}_j^{i+1}\,\tilde{A}_j^{i+1} + w_j^{i} A_j^{i}\right) = 0 \tag{4.14}$$

where

$$\tilde{w}_j^{i+1} = \begin{cases} \dfrac{K}{2h_j^{i+1}}\left[1 - \dfrac{\gamma^2 (h_j^{i+1})^2}{4|A_j^{i}|^2}\right] & ; \quad \dfrac{|A|}{h} > \dfrac{\kappa}{2} \text{ or already breaking} \\ 0 & \dfrac{|A|}{h} < \dfrac{\gamma}{2} \text{ or not yet broken} \end{cases} \tag{4.15}$$

If waves are unbroken in all j grid blocks, $\tilde{w}_j^{i+1}$ is set equal to zero and the scheme proceeds based on equation (4.14) with no second iteration.

4.4. Normally Incident Waves on a Plane Slope

Several cases were run for waves starting in a depth of 2 m and propagating directly towards shore over a plane slope. The program checks at each step that the wave height has not exceeded the breaking criterion. When H becomes greater than κh, the program begins calculating values of the damping coefficient (4.15). Breaking continues until w falls to a value of zero, which does not occur on the plane beaches studied here but would be expected to occur readily for waves propagating over uneven topography. For each case examined, the wave height was assumed to be 1.0 m at a depth of 2 m, and wave period was assumed to be 5 seconds. Values of α = 1, 3, and 10 were tested using various computational grid spaces Δx. Results for α = 1 and Δx = 0.2 m and 1.0 m are shown in Figure 4.3, α = 3 and Δx = 1.0, 2.0, and 5.0 m in Figure 4.4 and α = 10 and Δx = 2.0, 5.0 and 10.0 m in Figure 4.5. The exact solution (4.4) is included in each figure for comparison, with h_b being taken as the average of the depth at the last grid point before breaking and at the first grid point after breaking. In each case, the numerical results provide an adequate representation of the exact solution.

4.5. Application to Offshore Islands

Due to a complex combination of wave breaking, refraction and diffraction, the wave field in the vicinity of an offshore island, either natural or man-made, is extremely complicated. For pure refraction Pocinki (1950) has provided a solution, and for nonbreaking waves Jonsson et al. (1976) and Smith and Sprinks (1975) have developed solutions which include refraction and diffraction. However, an island will generally possess a surf zone and the shadow zone created behind the island will persist for longer distances than for the nonbreaking wave case due to loss of energy near the

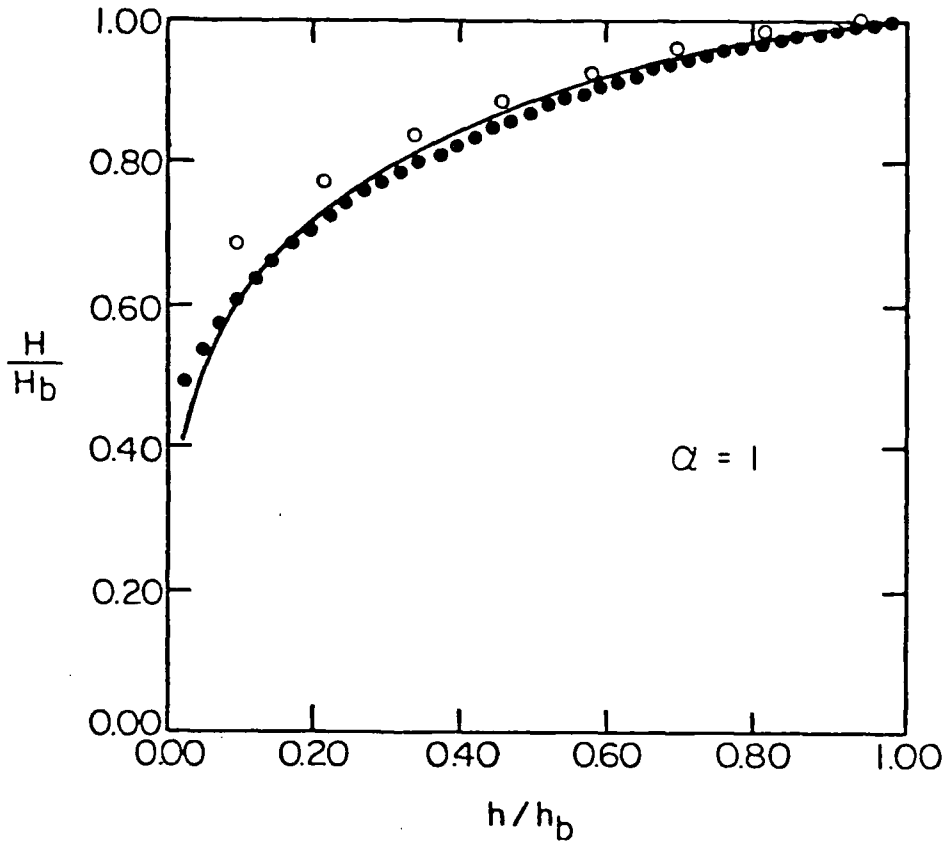

Figure 4.3. Numerical results for wave height decay; normal incidence. α = 1, s = 0.15. ——— analytic solution; •, Δx = 0.2 m; o, Δx = 1.0 m.

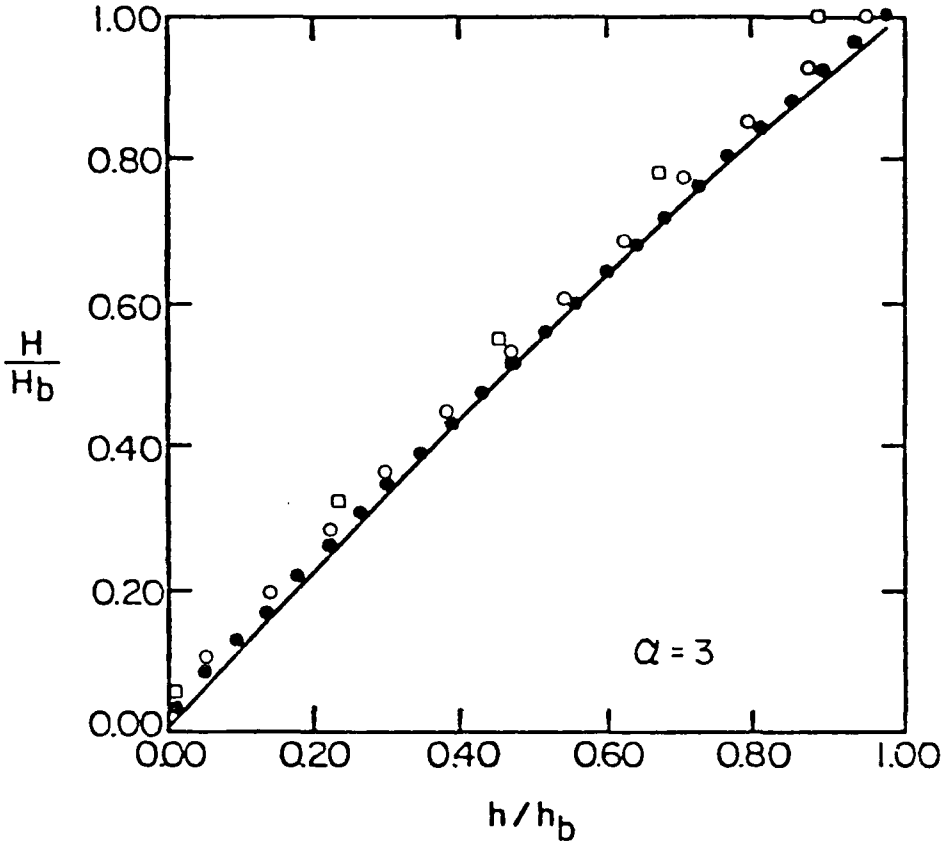

Figure 4.4. Numerical results for wave height decay; normal incidence. $\alpha = 3$, $s = 0.05$. ——— analytic solution; ●, $\Delta x = 1.0$ m; ○, $\Delta x = 2.0$ m; □, $\Delta x = 5.0$ m.

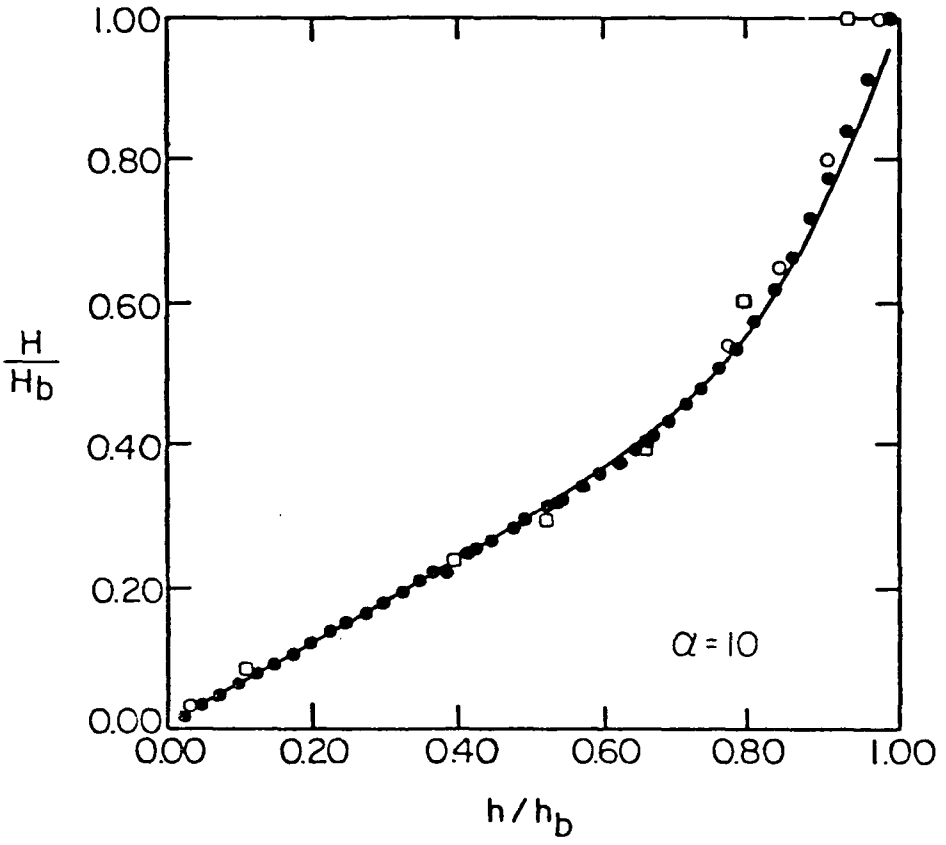

Figure 4.5. Numerical results for wave height decay; normal incidence. α = 10, s = 0.015. ——— analytic solution; ●, Δx = 2.0 m; ○, Δx = 5.0 m; □, Δx = 10.0 m.

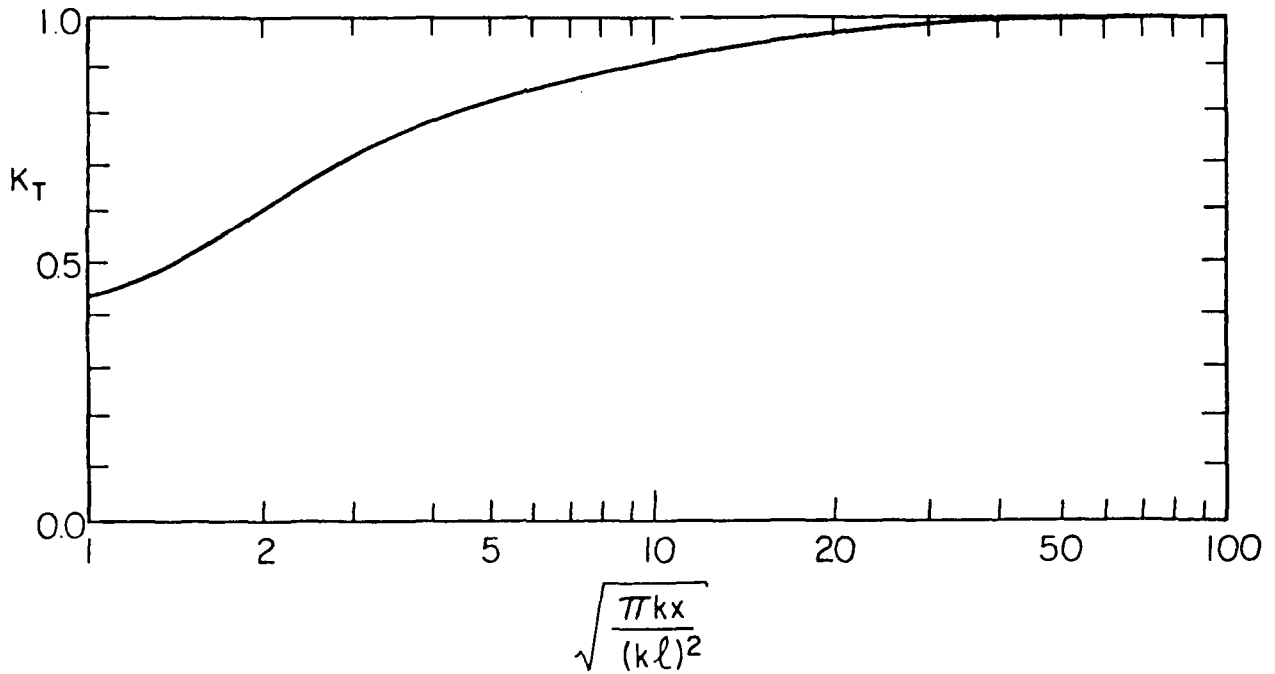

Figure 4.10. Transmission coefficient $|A(x,0)|$ along centerline y = 0.

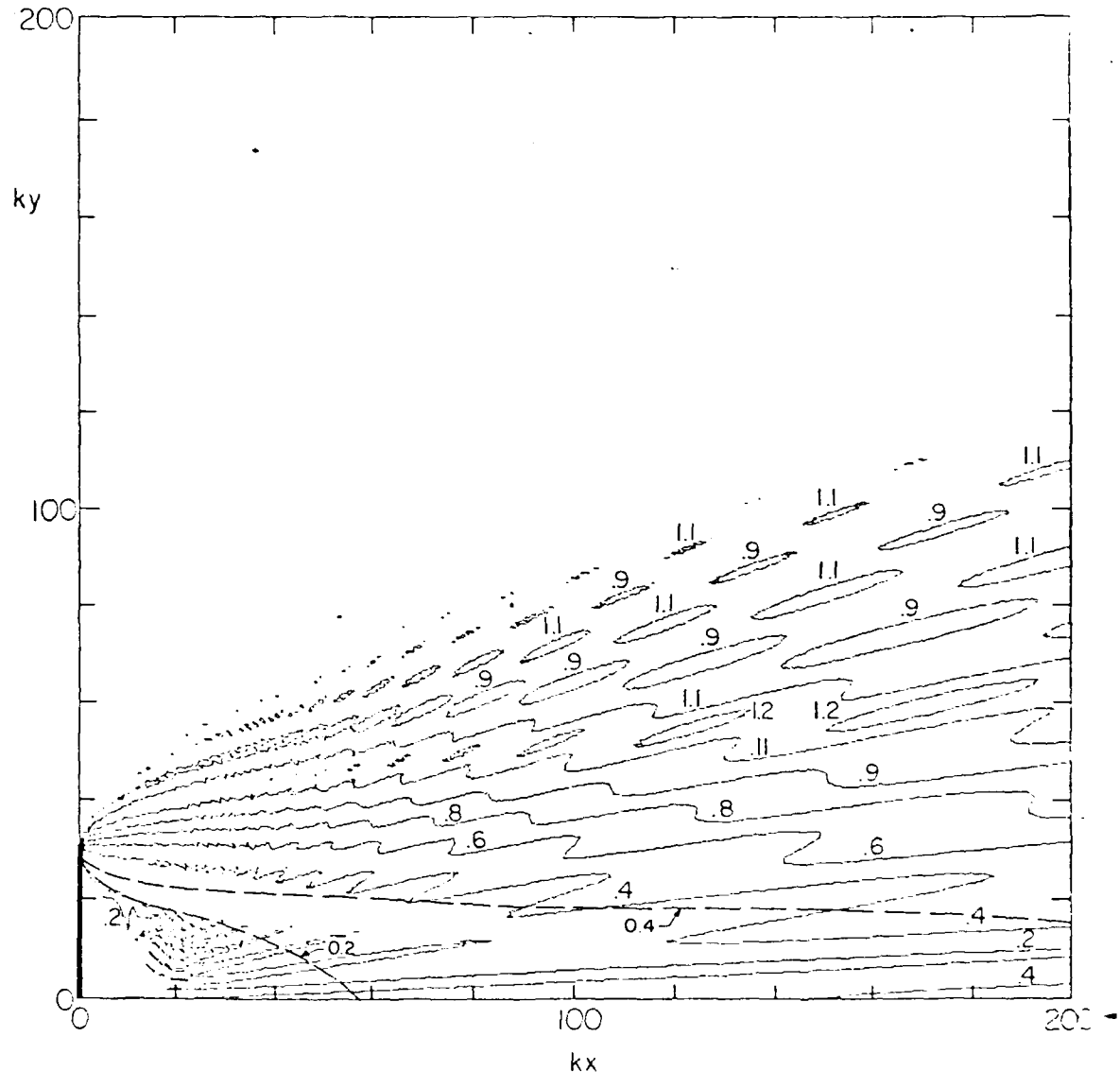

Figure 4.9. (Continued).

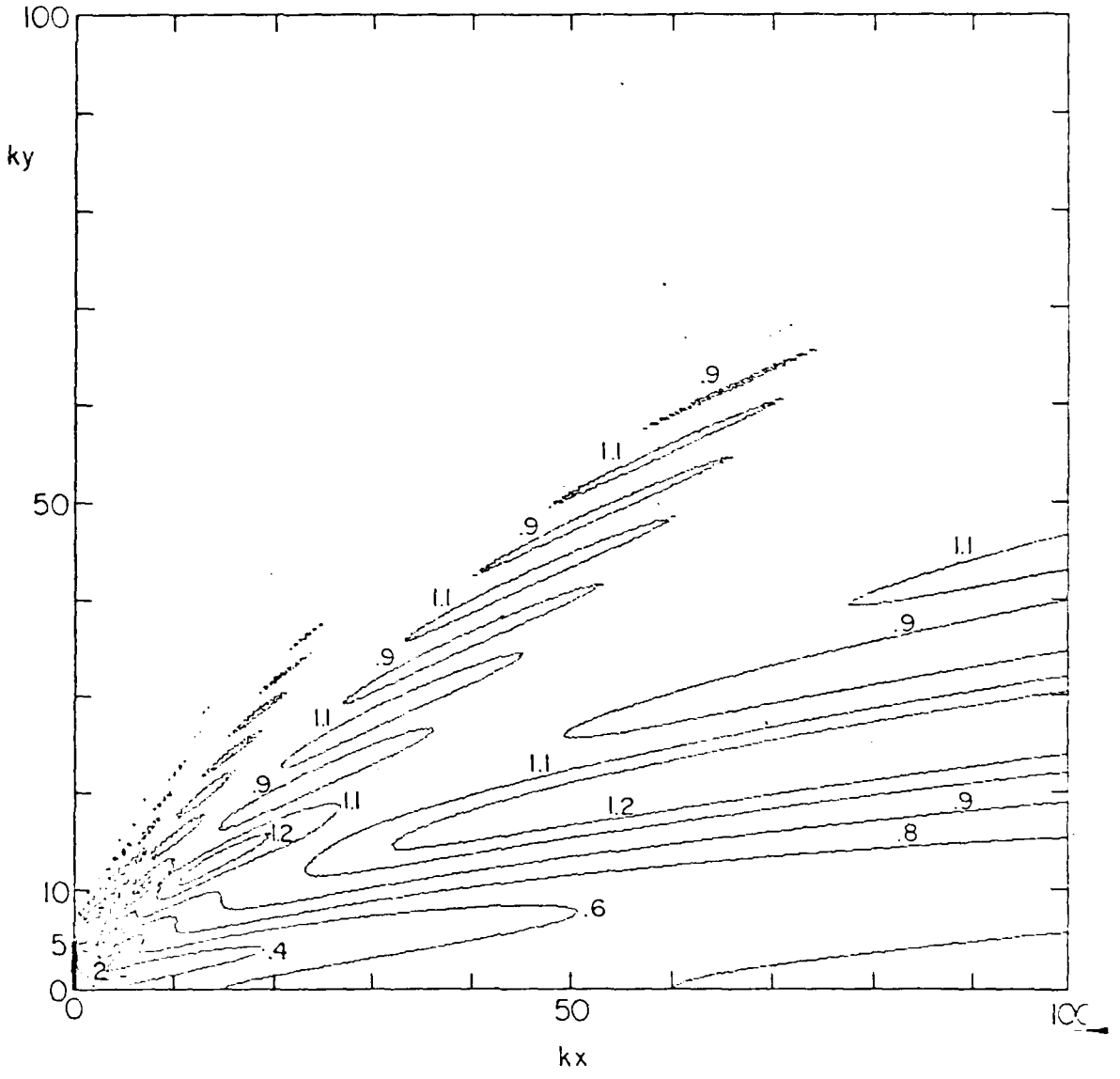

Figure 4.9. Transmission coefficient $|A(x,y)|$ behind short breakwater; a) $k\ell = 5$, b) $k\ell = 10\pi$ (example of Penney and Price, 1952), ---- Penney and Price results.

Downwave of the breakwater, the transmission coefficient is given by $k_T = |A(x,y)|$. In Figure 4.9a,b, several contour plots of k_T are provided for breakwaters with dimensionless widths of $k\ell = 5$ and 10π. Contrary to the situation shown in Penney and Price ($k\ell = 10\pi$, their Figure 7) which neglected the interaction between the diffraction patterns from each end of the breakwater, the minimum value of k_T does not occur directly behind the breakwater but off to each side along a parabolic curve due to the development of a short crested pattern of intersecting waves in the lee of the breakwater or island.

As a non-conservative measure of the extent of the shadow behind an island, we will use the centerline value ($y = 0$). Figure 4.10 shows k_T vs. $(\frac{\sqrt{\pi kx}}{k\ell})$. From the figure the transmission coefficient increases asymptotically to unity for large x as the waves diffract around the island. As an example, at a distance given by $kx = \frac{(9.3\ k\ell)^2}{\pi}$, the wave height recovers to 90% of its original value. Expressing x in terms of the width of the island, $x = x_{90} 2\ell$, where x_{90} is the dimensionless distance to the point where 90% of the original amplitude is recovered, we obtain $x_{90} = [\frac{(9.3)^2}{2\pi}] k\ell$. The distance x_{90} depends on the relative size of the island width to a wavelength; the wider the island the longer it takes for the wave height to recover. Note that for $k_T = 0.75$, the distance is far shorter, $x = x_{75}(2\ell) = \frac{(3.32)^2}{2\pi} k\ell(2\ell)$, which is about 8 times closer to the island. In practice, a factor of two or three should be applied to x, since, as shown, the minimum value of k_T is not directly behind the island.

4.7. Conclusion

A method for including the effect of wave breaking in parabolic models for combined refraction and diffraction has been developed and shown to give good agreement to laboratory results for wave heights acr the surface.

the model to the other, instead of infinity. For simple geometries, analytical solutions are available as a third way to compute the far-field wave heights. This latter course is chosen here to examine the waves behind an island approximated by an offshore breakwater.

By superposing the solutions of the LaPlace equation for normally incident waves propagating past a half-infinite breakwater, Penney and Price (1950) showed results of the transmission coefficient for an island with a width of 10 wavelengths. A similar superposition was done by Liu and Mei (1976) using a similar parabolic equation to the one treated here. An island with a small width to length ratio was examined by Mei and Tuck (1980). Here we develop an exact solution of the parabolic approximation for the normally incident wave field behind a short breakwater, in order to approximate the effect of an island totally blocking the incident wave. The solution is provided in Appendix II.

Defining $\alpha = \sqrt{k/\pi x}\ (y+\ell)$ and $\beta = \sqrt{k/\pi x}\ (y-\ell)$, where k is the wave number of the normally incident wave, 2ℓ as the width of the breakwater, and x as the downwave direction, the normalized wave amplitude is

$$A(x,y) = 1 - \left(\frac{1-i}{2}\right)[C(\alpha) - C(\beta) + i(S(\alpha) - S(\beta))] \qquad (4.19)$$

where C(x), S(x) are the Fresnel cosine and sine integrals:

$$C(x) = \int_0^x \cos(\pi t^2/2)dt \qquad (4.20)$$

$$S(x) = \int_0^x \sin(\pi t^2/2)dt \qquad (4.21)$$

$$|A^*|_j^{i+1} = \alpha|A|_{j-1}^{i+1} + (1-2\alpha)|A|_j^{i+1} + \alpha|A|_{j+1}^{i+1} \qquad (4.17)$$

where α was taken as 0.2. This filter successfully eliminated noise but interacted with the breaking wave model to the extent that the overall form of the solution differed. Instead, we employ a scheme in which the model searches for anomalously large values of A occurring along grid rows with a contracting surfzone and reduces the large values in magnitude to a value equal to the water depth. The plots in Figures 4.6-8 present unfiltered data in order to give an idea of the magnitude of the remaining noise and its effect on the overall contours.

4.6. The Far-Field of the Island

The persistence of the shadow in the wave field behind the island is often an important variable, particularly when siting an island near developed shorelines. In order to determine the wave field many wave lengths past the island, several procedures may be followed. First, the model can be run for longer distances than shown in Figures 4.6-8. Alternatively, the numerical model can be used as input to an analytical model, resulting in a hybrid model. This can be done using a convolution integral developed in the Appendix to determine A(x,y) over a region of constant depth.

$$A(x-\xi,y) = \sqrt{\frac{k}{2\pi(x-\xi)}}\, e^{-i\frac{\pi}{4}} \int_{-\infty}^{\infty} f(\zeta) e^{i\frac{k(y-\zeta)^2}{2(x-\xi)}}\, d\zeta \qquad (4.18)$$

where $f(\zeta)$ is the variation of A(x,y) along $x = \xi$, the last grid row in the numerical model. This integral is limited, of course, to the width of the numerical model and hence the integral is taken from one lateral boundary of

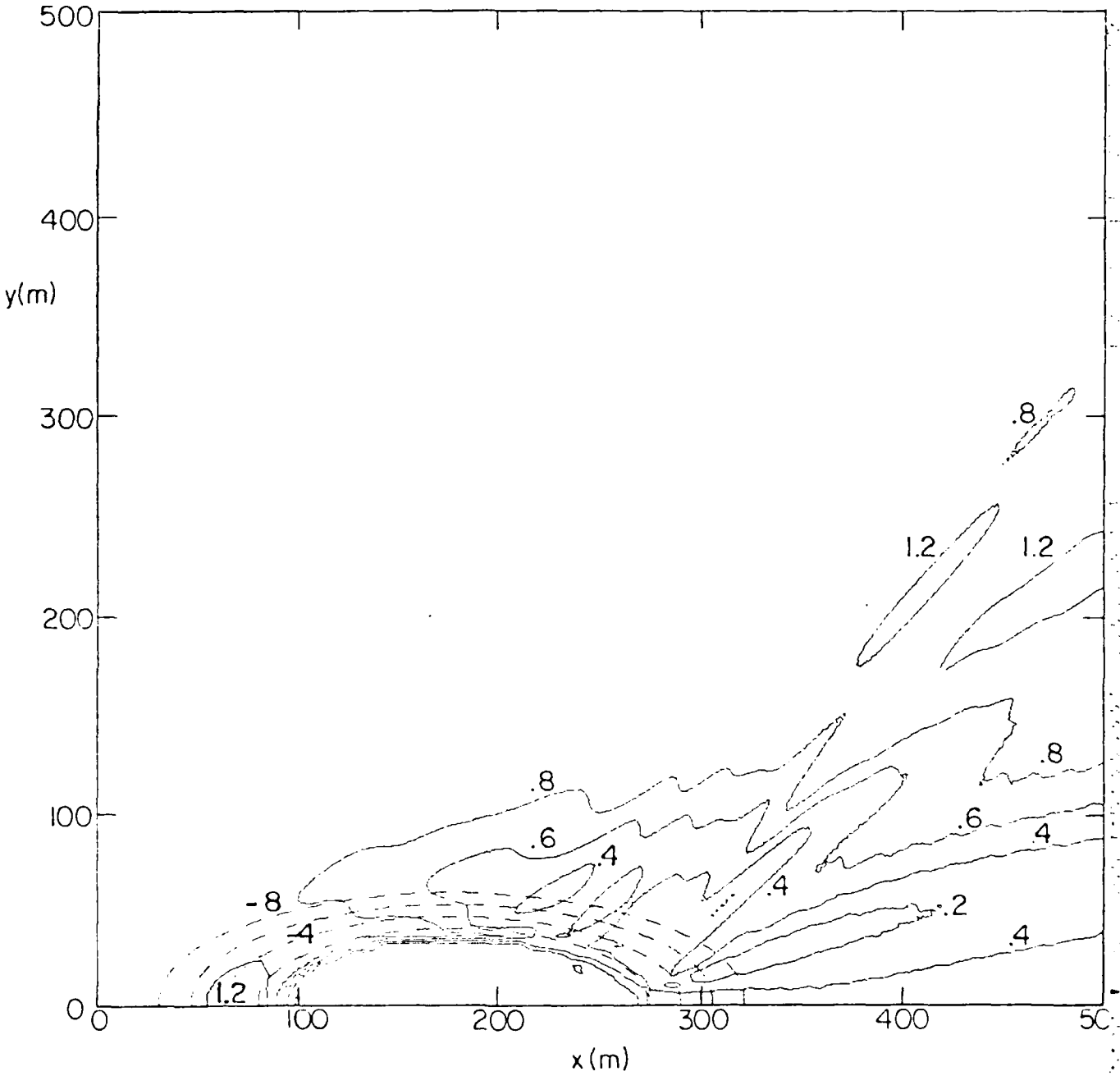

Figure 4.8. (Continued).

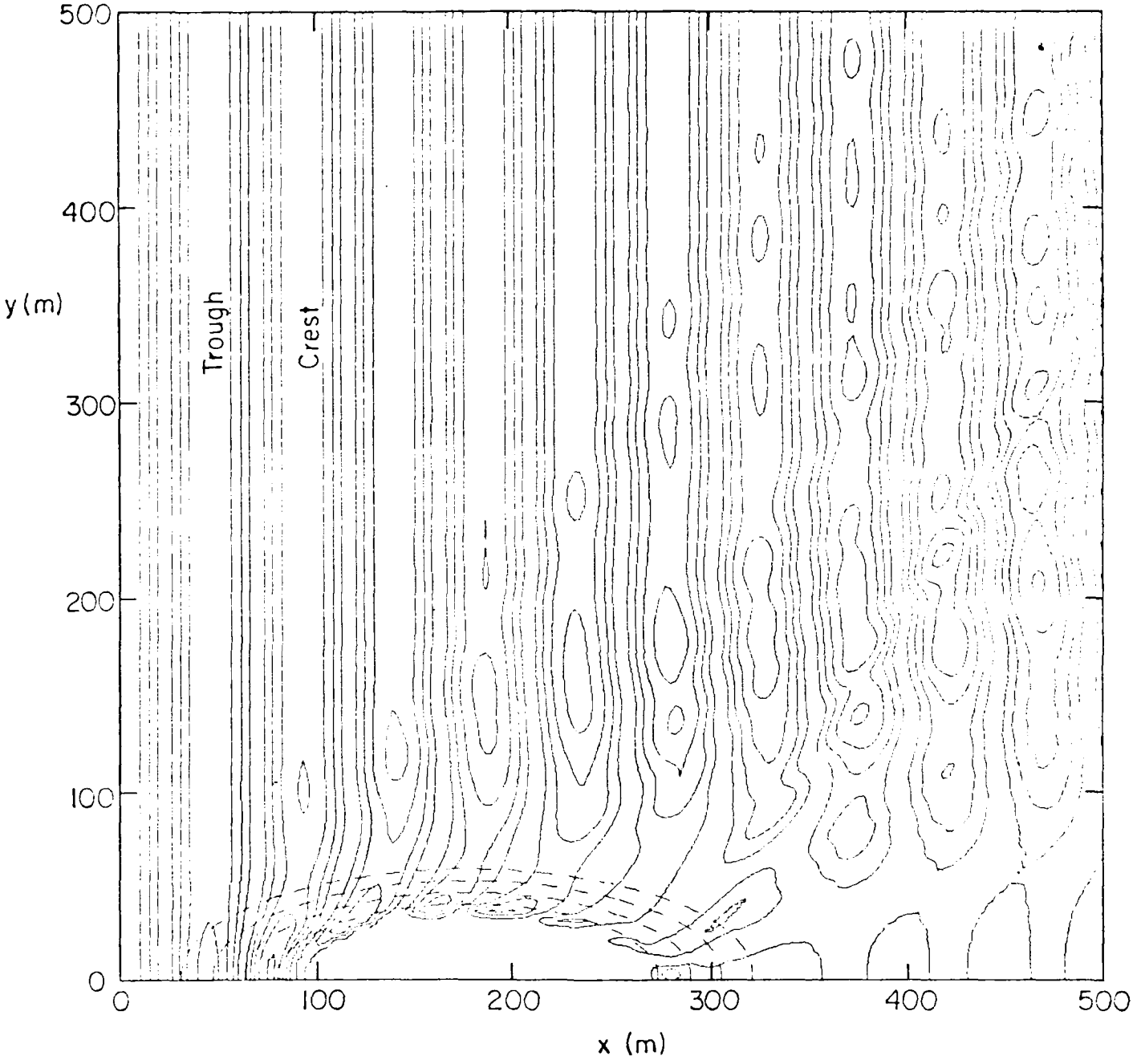

Figure 4.8. Elliptic island X_A = 160 m, Y_A = 60 m. a) Instantaneous surface contours. b) Wave height contours, $k_T = |A(x,y)|$.

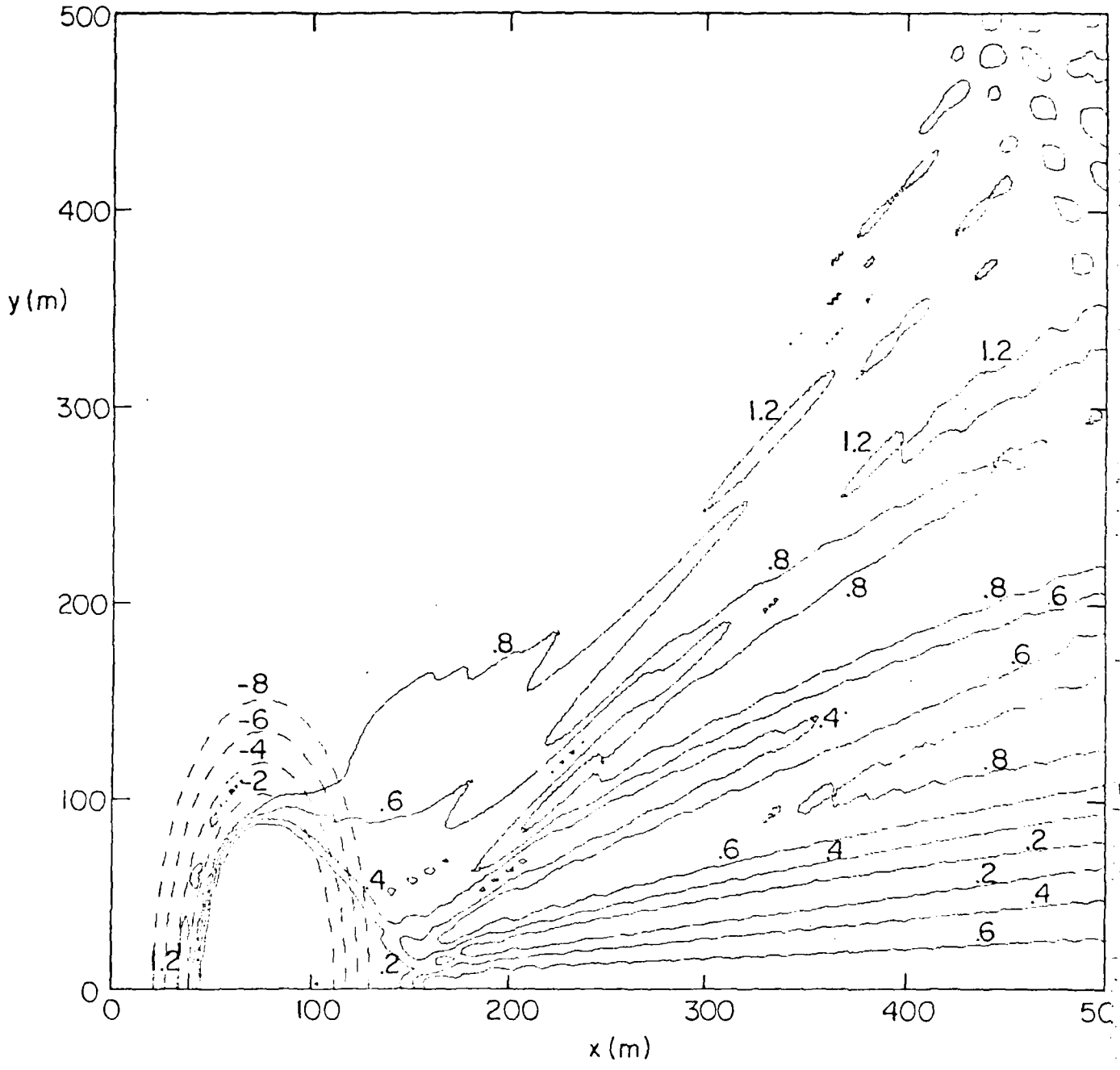

Figure 4.7. (Continued).

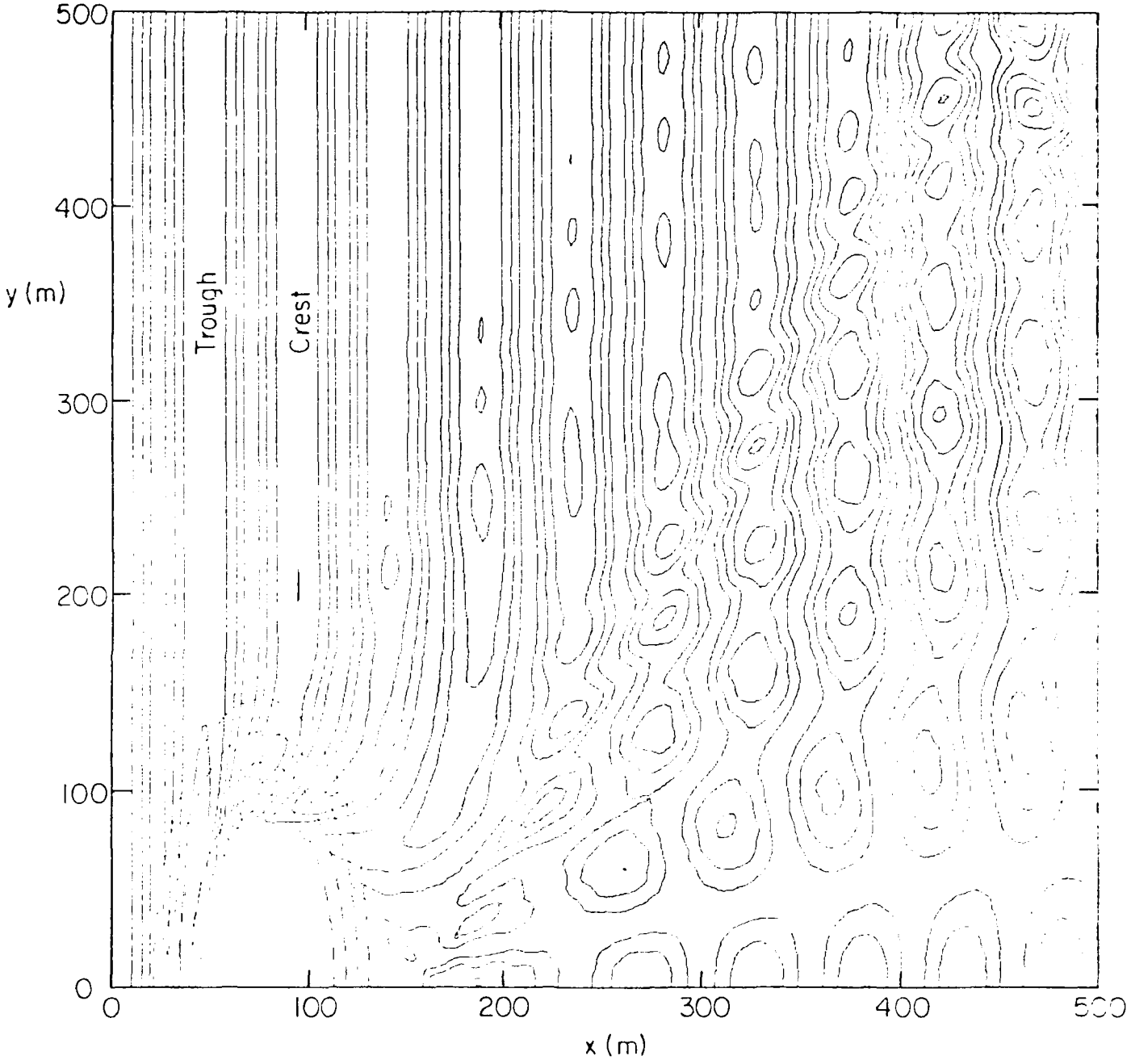

Figure 4.7. Elliptic island, X_A = 60 m, Y_A = 160 m. a) Instantaneous surface contours. b) Wave height contours, $k_T = |A(x,y)|$.

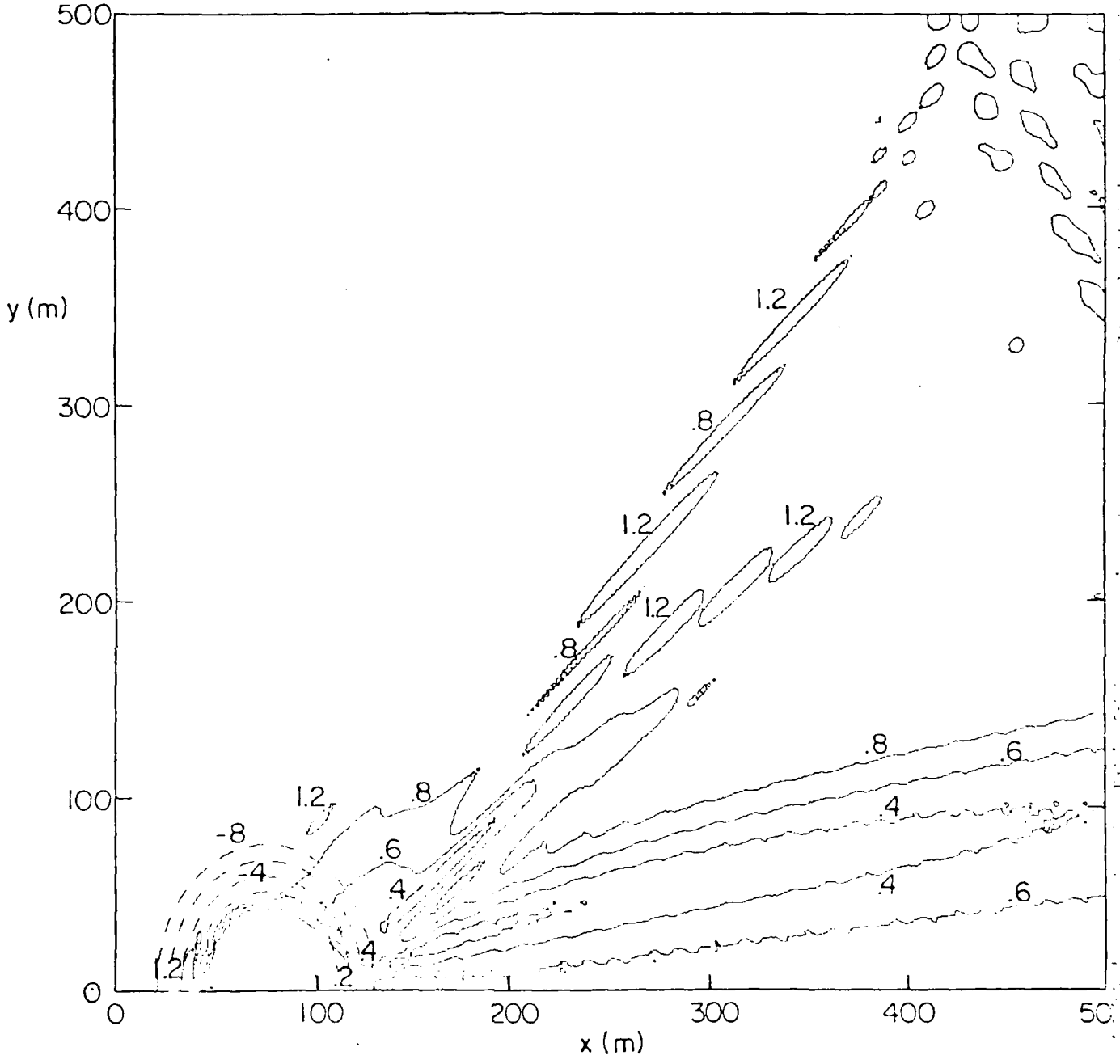

Figure 4.6. (Continued).

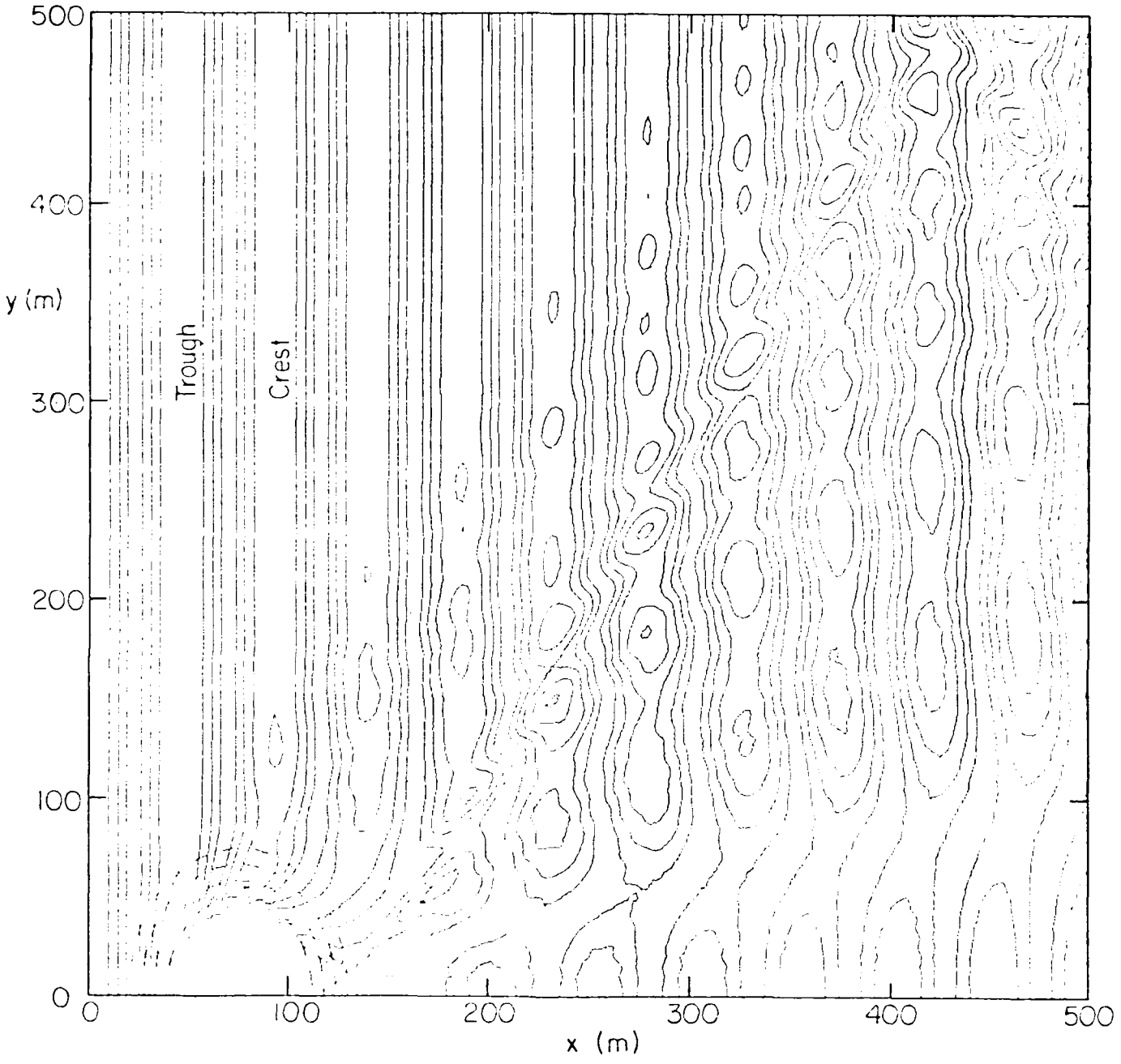

Figure 4.6. Elliptic island, X_A = 60 m, Y_A = 80 m. a) Instantaneous surface contours. b) Wave height contours, $k_T = |A(x,y)|$.

where h_b is the maximum height of the conical island above the bottom and X_A and Y_A are the semi-major axes of the ellipse measured at the bottom. The island's beach slopes vary with position around the island; but on the semi-major axes, it is h_b/X_A and h_b/Y_A.

For the computations, h_b = 20 m and X_A and Y_A vary. The incident wave has an amplitude of 1 m and a period of 10 seconds. The wave direction is assumed to be along the x-axis and the problem is symmetric about the x-axis, so only half the wave field is computed for this case. Figures 4.6, 4.7 and 4.8 show contour plots of the instantaneous water surface and the transmission coefficient around a nearly circular island (X_A = 60, Y_A = 80 m), a wide island (X_A = 60, Y_A = 160 m) and a long narrow island (X_A = 160, Y_A = 60 m). From the figures, which show approximately four wavelengths, it is clear that the shape of the island is extremely influential on the wave field behind the island, with the island with the smallest aspect ratio creating the smaller shadow. Additionally, the presence of the island creates a "bow-wave"-like disturbance which spreads laterally in the downwave direction. The refraction of the waves on the front side of the island creates a region of high wave height on the shoulders of the islands for all three cases. Further focusing of the wave behind the island occurs due to refraction by the island's bathymetry.

In practice, the shift from broken wave amplitudes to unbroken wave amplitudes along a y-grid row introduces a numerical discontinuity in the solution. This discontinuity introduces noise in the computed solution which then propagates into the downwave region. The noise is manifested as a stable Nyquist-wavenumber oscillation with an amplitude of about one to two percent of the initial wave amplitude. An attempt was made to numerically filter the oscillation during model calculations by the use of a dissipative interface in the surfzone on the updated row:

island boundary. Several numerical (two-dimensional) examples of waves in the vicinity of islands have been computed here using Eqns. (4.11) and (4.14) and including wave breaking.

The inclusion of dry shoreline boundaries or vertical walls in the computational domain of a wave model generally requires a modification of the domain which can include the specification of stair-step boundaries in the case of complicated obstacles. However, if the surface-piercing obstacle consists of a sloping structure which is expected to be surrounded by a surfzone, a major simplification may be introduced. By replacing the surface-piercing island by a shoal with a flat top and covered by a thin layer with a depth on the order of a centimeter, the entire island area may be included in the unmodified computational grid. In this "thin film" model, wave breaking then reduces wave height across the surfzone to a small value at the "real" shoreline, after which further breaking reduces the height of a wave propagating over the island to approximately γ times the film depth. This wave is transmitted beyond the island and plays no role in the downwave region due to its small height. This approach alleviates the need for internal grid boundaries unless reflective structures are to be included.

The islands in the present computations have an elliptical planform, and are located in water of constant depth h_o = 10 m. The depth contours of the islands are given by

$$h = \begin{cases} h_b \left(\sqrt{\left(\frac{X}{X_A}\right)^2 + \left(\frac{Y}{Y_A}\right)^2} - 1 \right) + h_o \quad ; \\ \qquad \text{for } \left(\frac{X}{X_A}\right)^2 + \left(\frac{Y}{Y_A}\right)^2 < 1 \\ h_o \quad ; \quad \text{for } \left(\frac{X}{X_A}\right)^2 + \left(\frac{Y}{Y_A}\right)^2 > 1 \end{cases} \tag{4.16}$$

The "thin film" model provides a convenient means to predict the wave heights in the vicinity of an island without the computational necessity of including internal boundary conditions to the model. Islands are treated as extremely shallow shoals and wave breaking insures that these "thin film" shoals produce wave patterns equivalent to those for a surface-piercing island.

The shadow thrown by islands in the downwave direction persists for distances equivalent to many island widths, depending on the dimensionless island width ($k\ell$). An analytic model for constant depth is developed to illustrate the diffracted wave field behind the island.

There exists a general absence of data on the characteristics of breaking waves propagating either normally or obliquely over arbitrarily uneven topography. Thus, many of the predictions of the present model are necessarily qualitative in nature, and require further verification which depends on the future availability of data.

Appendix 4.1. Analytic Solution for the Constant-Depth Half-space

Over a flat bottom, neglecting dissipation, the parabolic equation for the wave amplitude, $A(x,y)$, behind the island is

$$2ik \frac{\partial A}{\partial x} + \frac{\partial^2 A}{\partial y^2} = 0$$

[illegible] is the wave number. This equation may be used to extend the results [illegible]ously described finite-difference calculations to the farfield of [illegible]r similar obstacle). The boundary condition (obtained at the [illegible] the computational grid) may be taken as

$$A(0,y) = f(y) \quad ; \quad |y| < \infty$$

where now x = 0 signifies the start of the half-space to be considered. Using the Fourier transform pair:

$$\hat{A} = \int_{-\infty}^{\infty} A(x,y)e^{-i\lambda y}dy \quad ; \quad A = \frac{1}{2\pi}\int_{-\infty}^{\infty} \hat{A}(x,\lambda)e^{i\lambda y}d\lambda \ ,$$

we obtain an equation in x alone,

$$2ik\frac{\partial \hat{A}}{\partial x} - \lambda^2\hat{A} = 0$$

where

$$\hat{A}(0,\lambda) = \hat{f}(\lambda) = \int_{-\infty}^{\infty} f(y)e^{-i\lambda y}dy$$

Solving, we obtain

$$\hat{A}(x,\lambda) = \hat{A}(0,\lambda)e^{\lambda^2 x/2ik}$$

This solution may be used in either continuous form or in a discretized form using FFT methods to extend the finite-difference calculations. Here, we consider a special case of a breakwater of length 2ℓ situated on the y-axis at x = 0. For the general case of waves obliquely incident on x = 0, f(y) may be written as

$$f(y) = \begin{cases} 0 & ; \quad |y| < \ell \\ e^{i\lambda_o y} & ; \quad |y| > \ell \end{cases}$$

where λ_o is the y-component of the wavenumber vector

$$\lambda_o = k\sin\theta$$

Transforming f(y) gives

$$\hat{A}(0,\lambda) = 2\pi\delta(\lambda_o-\lambda) - \frac{2\sin(\lambda_o-\lambda)\ell}{(\lambda_o-\lambda)}$$

where δ is the Dirac delta function.

Taking the inverse transform of $\hat{A}$ gives

$$A(x,y) = \frac{1}{2\pi}\int_{-\infty}^{\infty}\left[2\pi\delta(\lambda_o-\lambda) - \frac{2\sin(\lambda_o-\lambda)\ell}{(\lambda_o-\lambda)}\right]e^{-i\lambda^2 x/2k}e^{i\lambda y}d\lambda$$

$$= e^{-i\lambda_o^2 x/2k}\,e^{i\lambda_o y} - \sqrt{\frac{k}{2\pi x}}\,e^{-i\pi/4}\int_{-\ell}^{\ell} e^{i\lambda_o\zeta}e^{ik(y-\zeta)^2/2x}d\zeta$$

where the first term represents an undisturbed, obliquely-oriented plane wave and the second term contains the disturbance due to the breakwater. Setting λ_o equal to zero (normal incidence) and introducing the definitions of the Fresnel cosine and sine integrals yields equation (4.17). The solutions obtained using the parabolic approximation are similar in form to the form of the Fresnel approximation in optics.

References

Battjes, J. A., and Janssen, J.P.F.M., 1978, "Energy loss and set-up due to breaking of random waves," Proc. 16th I.C.C.E., 569-587.

Berkhoff, J. C. W., 1972, "Computation of combined refraction-diffraction," Proc. 13th Int. Conf. Coastal Engrg., Vancouver.

Berkhoff, J. C. W., Booij, N., and Radder, A. C., 1982, "Verification of numerical wave propagation models for simple harmonic linear water waves," Coastal Engng., 6, 255-279.

Booij, N., 1981, "Gravity waves on water with non-uniform depth and current," Report No. 81-1, Dept. of Civil Engineering, Delft University of Technology.

Chu, H.-L., 1975, "Numerical model for wave refraction by finite amplitude wave theories," ASCE, Symp. on Modelling Techniques, San Francisco, CA, 1082-1100.

Dally, W. R., Dean, R. G., and Dalrymple, R. A., 1984, "A model for breaker decay on beaches," ASCE, 19th Int. Conf. on Coast. Engng., Houston, TX.

Dally, W. R., Dean, R. G., and Dalrymple, R. A., 1984, "Modeling wave transformation in the surf zone," Misc. Paper CERC-84-8 U.S. Army Coastal Engineering Research Center, Vicksburg.

Dalrymple, R. A., Kirby, J. T., and Hwang, P. A., 1984, "Wave diffraction due to areas of energy dissipation," J. Waterway, Port, Coastal and Ocean Engrg., 110, 67-79.

Dean, R. G., 1965, "Stream function representation of nonlinear ocean waves," J. Geophys. Res., 70, 4561-4577.

Dingemans, M. W., 1983, "Verification of numerical wave propagation models with field measurements," Rept. W488 Part 1, Delft Hydraulics Laboratory.

Dingemans, M. W., Stive, M. J. F., Kuik, A. J., Radder, A. C. and Booij, N., 1984, "Field and laboratory verification of the wave propagation model CREDIZ," Proc. 19th Intl. Conf. Coastal Engrng., Houston.

Divoky, D., LeMehaute, B., and Lin, A., 1970, "Breaking waves on gentle slopes," J. Geophys. Res., 75, 1681-1692.

Ebersole, B. A., and Dalrymple, R. A., 1980, "Numerical modelling of nearshore circulation," Proc. 17th Int. Conf. Coastal Engineering, Sydney.

Flick, R. E., 1978, "Study of shoaling waves in the laboratory," Ph.D. dissertation, University of California, San Diego.

Goring, D. G., 1978, "Tsunamis - the propagation of long waves onto a shelf," Rept. No. KH-R-38, W. M. Keck Laboratory, California Institute of Technology.

Headland, J. R., and Chu, H.-L., 1984, "A numerical model for refraction of linear and cnoidal waves," Proc. 19th Int. Conf. Coastal Engineering, Houston, Texas.

Hedges, T. S., 1976, "An empirical modification to linear wave theory," Proc. Inst. Civ. Engrs., 61, 575-579.

Horikawa, K., and Kuo, C.-T., 1966, "A study of wave transformation inside surfzone," Proc. 10th Int. Conf. Coastal Engrg., Tokyo, 217-233.

Jonsson, I. G., Skovgaard, O., and Brink-Kjaer, O., 1976, "Diffraction and refraction calculations for waves incident on an island, J. Mar. Res., 34, 469-496.

Kirby, J. T., 1983, "Propagation of weakly-nonlinear surface water waves in regions with varying depth and current," Rept. CE-83-37, Dept. of Civil Engng., University of Delaware, Newark, DE.

Kirby, J. T., 1984, "A note on linear surface wave-current interaction over slowly varying topography," J. Geophys. Res., 89, 745-747.

Kirby, J. T., and Dalrymple, R. A., 1983a, "A parabolic equation for the combined refraction-diffraction of Stokes waves by mildly varying topography," J. Fluid Mech., 136, 453-466.

Kirby, J. T., and Dalrymple, R. A., 1983b, "Propagation of weakly nonlinear surface waves in the presence of varying depth and current," Proc. 20th Congr. IAHR, Moscow, Vol. 7, 198-202.

Kirby, J. T., and Dalrymple, R. A., 1984, "Verification of a parabolic equation for propagation of weakly-nonlinear waves," Coastal Engineering, 8, 219-232.

Liu, P.L-F., 1984, "The effect of friction on the evolution of Stokes waves," manuscript.

Liu, P. L-F., and Mei, C. C., 1976, "Water motion on a beach in the presence of a breakwater, I. Waves," J. Geophys. Res., 81, 3079-3084.

Liu, P. L-F., and Tsay, T. K., 1983, "On weak reflection of water waves," J. Fluid Mech., 131, 59-71.

Liu, P. L-F., and Tsay, T. K., 1984, "Refraction-diffraction model for weakly nonlinear water-waves," J. Fluid Mech., 141, 265-274.

Liu, P. L.-F., Yoon, S. B., and Kirby, J. T., 1985, "Nonlinear refraction-diffraction of waves in shallow water," J. Fluid Mech.,to appear.

Longuet-Higgins, M. S., 1970, "Longshore currents generated by obliquely incident sea waves 1," J. Geophys. Res., 75, 6778-6789.

Longuet-Higgins, M. S., and Stewart, R. W., 1963, "A note on wave set-up," J. Mar. Res., 21, 4-10.

Mei, C. C., and Tuck, E. O., 1980, "Forward scattering by thin bodies," S.I.A.M. J. Appl. Math., 30, 178-191.

Penney, W. G., and Price, A. T., 1952, "The diffraction theory of sea waves and the shelter afforded by breakwaters," Phil. Trans., Roy. Soc., London A 244, 236-253.

Pocinki, L. S., 1950, "The application of conformal transformations to ocean wave refraction problems," Trans. Amer. Geophys. Union, 31(6), 856-866.

Radder, A. C., 1979, "On the parabolic equation method for water wave propagation," J. Fluid Mech., 95(1), 159-176.

Rienecker, M. M. and Fenton, J. D., 1981, "A Fourier approximation method for steady water waves," J. Fluid Mech., 104, 119-137.

Skovgaard, O., and Petersen, H. M., 1977, "Refraction of cnoidal waves," Coastal Engineering, 1, 43-61.

Smith, R., and Sprinks, T., 1975, "Scattering of surface waves by a conical island," J. Fluid Mech., 72(2), 373-384.

Walker, J. R., 1976, "Refraction of finite-height and breaking waves," Proc. 15th Int. Conf. on Coastal Engng., Honolulu, HI.

Yue, D. K.-P., and Mei, C. C., 1980, "Forward diffraction of Stokes waves by a thin wedge," J. Fluid Mech., 99, 33-52.

Distribution

Office of Naval Research
Coastal Science Program
Code 42205
Arlington, VA 22217

Defense Documentation Center
Cameron Station
Alexandria, VA 22314

Director, Naval Research Lab.
ATTN: Technical Information Officer
Washington, D. C. 20375

Director
Office of Naval Research Branch Office
1030 East Green Street
Pasadena, CA 91101

Chief of Naval Research
Code 100M
Office of Naval Research
Arlington, VA 22217

Office of Naval Research
Operational Applications Division
Code 200
Arlington, VA 22217

Office of Naval Research
Scientific Liaison Officer
Scripps Institution of Oceanography
La Jolla, CA 92093

Director Naval Research Laboratory
ATTN: Library, Code 2628
Washington, D. C. 20375

ONR Scientific Liaison Group
American Embassy - Room A-407
APO San Francisco, CA 96503

Commander
Naval Oceanographic Office
ATTN: Library, Code 1600
Washington, D. C. 20374

Naval Oceanographic Office
Code 3001
Washington, D. C. 20374

Chief of Naval Operations
OP 987P1
Department of the Navy
Washington, D. C. 20350

Oceanographer of the Navy
Hoffman II Building
200 Stovall Street
Alexandria, VA 22322

Naval Academy Library
U. S. Naval Academy
Annapolis, MD 21402

Commanding Officer
Naval Coastal Systems Laboratory
Panama City, FL 32401

Director
Coastal Engineering Research Center
U. S. Army Corps of Engineers
Kingman Building
Fort Belvoir, VA 22060

Officer in Charge
Environmental Research Prodctn Felty.
Naval Postgraduate School
Monterey, CA 93940

Director
Amphibious Warfare Board
U. S. Atlantic Fleet
Naval Amphibious Base
Norfolk, Little Creek, VA 23520

Commander, Amphibious Force
U. S. Pacific Fleet
Force Meteorologist
Comphibpac Code 25 5
San Diego, CA 93155

Librarian, Naval Intelligence
Support Center
4301 Suitland Road
Washington, D. C. 20390

Commanding Officer
Naval Civil Engineering Laboratory
Port Hueneme, CA 93041

Chief, Wave Dynamics Division
USAE-WES
P. O. Box 631
Vicksburg, MS 31980

Commandant
U.S. Coast Guard
ATTN: GECV/61
Washington, D.C. 20591

Office of Research and Development
%DS/62
U.S. Coast Guard
Washington, D.C. 20591

National Oceanographic Data
Center %D764
Environmental Data Services
NOAA
Washington, D.C. 20235

Dr. Edward Thornton
Department of Oceanography
Naval Postgraduate School
Monterey, CA 93940

Dr. Douglas I. Inman
University of California A-009
Shore Processes Laboratory
La Jolla, CA 92093

Dr. Dennis Conlon
ONR Detachment Code 422 CS
Arlington, VA 22217

END

FILMED

4-85

DTIC